Study of Slow Dynamics in Supercooled Water by Molecular Dynamics and Quasi-Elastic Neutron Scattering

by

Li Liu

Submitted to the Department of Nuclear Science and Engineering
in partial fulfillment of the requirements for the degree of
Doctor of Philosophy in Nuclear Science and Engineering
at the
MASSACHUSETTS INSTITUTE OF TECHNOLOGY
September 2005

Author .....
Department of Nuclear Science and Engineering
August 31, 2005

Certified by .....
Sow-Hsin Chen
Professor of Nuclear Science and Engineering
Thesis Supervisor

Read by .....
Sidney Yip
Professor of Nuclear Science and Engineering,
and Materials Science and Engineering
Thesis Reader

Read by .....
Dr. Chun(-Keung) Loong
Senior Physicist, Argonne National Laboratory
Thesis Reader

Accepted by .....
Jeffrey A. Coderre
Associate Professor of Nuclear Science and Engineering,
Chairman, Department Committee on Graduate Students

Study of Slow Dynamics in Supercooled Water by Molecular Dynamics and Quasi-Elastic Neutron Scattering

by

Li Liu

Submitted to the Department of Nuclear Science and Engineering
on August 31, 2005, in partial fulfillment of the
requirements for the degree of
Doctor of Philosophy in Nuclear Science and Engineering

Abstract

The slow dynamics of supercooled water is studied by modelling the spectrum of test particle fluctuations: intermediate scattering function (ISF). The theoretical models are compared with experimental measurements by quasi-elastic neutron scattering (QENS) and molecular dynamics (MD) simulation results.

The dynamics of supercooled water can be decoupled into a product of translational and rotational dynamics. While the translational dynamics is modelled well by a product of a ISF representing short time in-cage vibrations and long time cage relaxation processes, the rotational dynamics is an aspect we shall study in this thesis. We introduce a model for the first, second and third order rotational correlation functions, which are required for the computation of the rotational intermediate scattering function corresponding to the incoherent QENS spectra from supercooled water. The model is tested against MD data generated from an extended-simple-point-charge (SPC/E) model of water and is found to be satisfactory. The analysis can be used as a practical method for extracting rotational relaxation parameters from QENS spectra measured at large Q from supercooled bulk water or interfacial water in porous materials.

By confining water in nano-pores of silica glass, we can bypass the crystallization and study the pressure effect on the dynamical behavior in deeply supercooled state using incoherent QENS technique.

we investigated the dynamics of water confined in nanoporous alumino-silicate matrices, from ambient temperature to the deeply supercooled state. We collected data on three instruments, with widely different resolutions, the Fermi chopper (FCS), the disk chopper (DCS) and the backscattering (HFBS) spectrometers at the NIST Center for Neutron Research (NIST NCNR). The confining systems were lab synthesized nanoporous glasses MCM-41-S and MCM-48-S. Inside the pores of these matrices the freezing process of water is retarded so that freezing occurs at a temperature about 50 K less than in bulk water. Thus, with the combined use of different instruments and nano-pore confinement, we were able to study the system over a wide temperature range, 160-325 K, with different energy resolutions. The data from all the three

spectrometers were analyzed using a single consistent expression based on the relaxing cage model (RCM) for the translational and rotational dynamics. A remarkable slowing down of the translational and rotational relaxation times has been observed.

The behavior of shear viscosity η or equivalently the structural relaxation time τ of a supercooled liquid as it approaches the glass transition temperature is called 'fragile' if it exhibits non-Arrhenius character, such as that described by the Vogel-Fulcher-Tammann (VFT) law; otherwise, with η and τ obeying Arrhenius law, it is called 'strong'. The fragile behavior is typical to ionic and van der Waals systems. In contrast, a liquid being strong reflects that its structural makeup, to a large extent by strong (commonly covalent) bonds forming a network structure. Bulk water is considered as a fragile liquid at room temperature but for supercooled water, a 'fragile-to-strong' (F-S) transition at around 228 K has been proposed to occur at around 228 K, based on a thermodynamic argument. The F-S transition in a molecular liquid like water may be interpreted as a variant of kinetic glass transition predicted by the ideal Mode-Coupling Theory (MCT), where the real structural arrest transition is avoided by an activated hoping mechanism below the transition.

Experiments at DCS and HFBS for water in MCM-41-S with 14 Å pore diameter were also done under selective pressures, from ambient to 2400 bar. We observe a clear evidence of a cusp-like F-S dynamic transition at pressures lower than 1600 bar. Here we show that the transition temperature decreases steadily with an increasing pressure, until it intersects the homogenous nucleation temperature line of bulk water at a pressure of 1600 bar. Above this pressure, it is no longer possible to discern the characteristic feature of the F-S transition.

The discussion part of this thesis concludes that the high-temperature liquid corresponds to the high-density liquid (HDL) of which the hydrogen bond network is not fully developed to conform a locally tetrahedral coordination, while the low-temperature liquid corresponds to the low-density liquid (LDL) of which the more open, locally 4-coordinated, ice-like hydrogen bond network is fully developed. Identification of the end point of F-S transition with a possible second critical point is also discussed.

Thesis Supervisor: Sow-Hsin Chen
Title: Professor of Nuclear Science and Engineering

Acknowledgments

Special thanks go to my advisor Professor Sow-Hsin Chen. Without his insightful guidance, counsel, support and encouragement, any part of this thesis would not have been possible. Thanks also go to Professor Sidney Yip and Dr. Chun(-Keung) Loong for their thoughtful advice on my career and helpful information on the molecular dynamics theory, quasi-elastic neutron scattering and patience to read through the thesis. I also thank Professor Jianshu Cao for participating in my thesis committee and giving his advices.

Special thanks go to Dr. Antonio Faraone for continuous help and collaboration during the neutron scattering experiments and data analysis, Professor Chung-Yuan Mou and Chun-Wan Yen at National Taiwan University for supplying MCM samples, and Dr. Juscelino Leão for supplying the high pressure system for our experiments at National Institute of Standards and Technology (NIST).

Thanks are also due to Dr. Eugene Mamontov, Dr. Yimin Qiu, Dr. John R.D. Copley, Dr. Inma Peral, and Dr. Dan A. Neumann at NIST and Dr. Alexander Kolesnikov at Argonne National Laboratory (ANL) for the beam lines and assistance in my experiments, Professor Piero Baglioni at University of Florence, Professor Francesco Mallamace at University of Messina, and Professor H. Eugene Stanley at Boston University for their kindly advises and productive discussions.

Moreover, special thanks go to my husband Lingyun Li. Without his long-time support, any part of my study and research would not have been possible.

The friends I met at MIT have made my life here full of joy. I wish to thank my friends Yun Liu, Dazhi Liu, Matteo Broccio, Zhe Sun, Ciya Liao, Rong Wang, Wei-Ren Eric Chen, Xinyuan Chu, Hua Li...

Finally, this thesis is dedicated to all my family members: my most beloved mother and father, sister and brother-in-law, brother and sister-in-law, uncles, aunts, and cousins, ...

Contents

List of Figures

List of Tables

Chapter 1

Motivations for Research on Slow Dynamics of Supercooled Water

Water is essential for all living systems and the most abundant and important substance on Earth. From agriculture to travel, and from public health to commerce, the properties of water shape human activity and define the geography, topography, and environment in which we live. Indeed, life itself cannot exist without water [1].

Water can exist in many different condensed forms, 13 of which have been identified to date. Of those, nine are stable over some range of temperature and pressure – for example, at atmospheric pressure, ordinary hexagonal ice is stable between 72 and 273 K – and the other forms are metastable [2, 3, 4, 5]. Although the stable form of water at sufficiently high temperature is gas and sufficiently low temperature is inevitably crystalline, liquid water can also exist above its boiling temperature upon superheating and below its freezing temperature upon supercooling, down to approximately 235 K [6]. When those occur, water is said to be superheated or supercooled.

Supercooled water can be naturally produced in the form of small droplets in clouds and plays a key role in the processing of solar and terrestrial radiative energy fluxes. Supercooled water is also important for life at subfreezing conditions, for commercial preservation of proteins and cells, and for prevention of hydrate formation in natural gas pipelines [1].

1.1 Puzzling Behavior of Liquid Water and Plausibility Arguments

In the deeply supercooled region, strange things happen: a number of thermodynamic response functions of supercooled water, notably the isothermal compressibility K_T and the constant-pressure specific heat C_P, show a power-law divergence behavior at a singular temperature, experimentally determined to be 228 K at the ambient pressure [7, 8]. Concurrently, the transport properties, such as the shear viscosity η and the inverse self-diffusion constant D, diverge according to power-laws toward the same singular temperature [9, 10]. These experiments were pioneered by Angell and co-workers over the past 30 years [1, 4, 11, 12].

Since water is such a ubiquitous substance in living systems, the counterintuitive behavior in its supercooled state stimulates enormous interests in condensed matter physics, physical chemistry and biophysics communities for the past three decades.

The anomalies of the thermodynamic quantities can be rationalized by a hypothesis of a liquid-liquid phase transition which in turn suggests the existence of a second low-temperature critical point at about 228 K and at somewhat elevated pressure [14]. On the other hand, the transport coefficient anomalies are reminiscent of the dynamical behavior of a supercooled liquid near the so-called kinetic glass transition temperature, predicted by the Mode-Coupling theory (MCT) [13].

1.2 Special Interest in Confined Supercooled Water

Below the melting point at 273 K it is possible to supercool normal bulk water down to about 235 K, called homogenous nuclear temperature, below which crystallization occurs. It is also possible to rapidly quench small quantities of water at temperatures below 100 K to form amorphous solid water, that is, glassy water. Thus there is an experimental inaccessible temperature region for bulk supercooled water between

roughly 150 K and 235 K [15].

Search for the predicted [14] first-order liquid-liquid transition line and its end point, the second low-temperature critical point [1, 12] in water, has been hampered by intervention of the homogenous nucleation process, which takes place at 235 K at the ambient pressure. However, by confining water in nano-pores of mesoporous silica MCM-41-S with a mean cylindrical pore diameter of 14 Å, we are able to study the dynamical behavior of water extended to 160 K from ambient temperature without crystallization. Using high-resolution Quasi-Elastic Neutron Scattering (QENS) method and Relaxing-Cage Model (RCM) for the analysis, we determine the temperature and pressure dependences of the average translational relaxation time $\langle \tau_T \rangle$ for the confined supercooled water.

Confined water is of importance in biological systems and may also provide a means of entering into the inaccessible temperature region for bulk supercooler water. In certain geometrical confinements the water molecules are unable to form a crystalline structure; the water thus remains fluid and, like any other supercooled liquid, becomes increasingly viscous as the temperature approaches glass transition temperature T_g [15]. Therefore, the interests of the scientific community in the properties of water confined in nanoporous matrices at supercooled temperatures are twofold. On the one hand, confining water in nanometric cavities allows us to study water in deeply supercooled states. This temperature range is of fundamental importance to science of water. At ambient pressure, bulk liquid water shows an anomalous increase of thermodynamic quantities and an apparent divergent behavior of transport properties, on approaching the singular temperature $T_c = 228$ K [7], which lies below the homogenous nucleation temperature T_H. Thus, there is a lack of experimental data in this temperature range, which hampers the verification or the rejection of the different physical pictures proposed to explain the origin of the anomalous behavior of water. On the other hand, in many real life systems water is not in its bulk form but is located near surfaces or contained in small cavities. It is the case, for example, for water in rocks, in polymer gels, and in biological membranes [16]. In addition, the properties of water in porous silica glasses, such as Vycor, and silica gel, are relevant

in catalytic and separation processes. The above two lines of interests are obviously closely related, as the clarification of the fundamental properties of water is likely to be the key for understanding the behavior of many real systems. For example, in the case of enzymatic activity of protein, it has been found that the onset of protein dynamics is strongly correlated to the onset of orientational fluctuations that initiate structural rearrangements within the transient H-bond water network surrounding the protein [17, 18]. Therefore, the study of the dynamics of water confined in nano-pores as a function of temperature and pressure is relevant in understanding important effects in systems of interest to biology, chemistry, and geophysics [19, 20].

1.3 Previous Studies

Due to the facts mentioned above, both the structure and dynamics of water in confined geometries have been widely studied using molecular dynamics (MD) simulations and different experimental techniques. MD simulations of the extended-simple-point-charge (SPC/E) model of bulk water have furnished relevant results for understanding the dynamics of supercooled water [21, 22, 23, 24, 25]. From the analysis of these results, the Relaxing-Cage Model (RCM) for the translational and rotational dynamics of water at supercooled temperatures was developed [21, 22]. In addition, MD simulations of SPC/E water confined in silica nanopores have been carried out [26, 27]. The interaction between the hydrophilic surface and the water molecules has noticeable effects on the structure of the first and second layer of water near the pore surface [28]. As far as the dynamics is concerned, in confinement, water molecules are in the glassy state with very low mobility already at ambient condition. In general, the water molecules show a dynamics similar to that of supercooled water [26, 27] at a lower equivalent temperature of ~ 30 degrees [17, 29].

Experimentally, the structural properties of water at supercooled temperatures [30] and in confinement [31] were studied extensively using x-ray and neutron diffraction. The relaxational dynamics of water confined in mesoporous matrices were studied using dielectric spectroscopy [15, 32, 33, 34, 35, 36] and different nuclear magnetic

resonance (NMR) techniques [37, 38, 39, 40].

1.4 Methods for the Study

Quasi-elastic neutron scattering (QENS) and inelastic neutron scattering (INS) techniques offer many advantages for the study of single particle dynamics of water. The main reason is that the total scattering cross section of hydrogen is much larger than those of oxygen, silicon, and carbon. Furthermore, the neutron scattering of hydrogen atoms is mostly incoherent so that QENS spectra reflect, essentially, the self-dynamics of the hydrogen atoms in water. Combining this dominant cross section of hydrogen atoms with the use of spectrometers having different energy resolutions, we can study the self dynamics of water in a wide range of time scales, encompassing pico-second to tens of nano-seconds. In addition, investigating different Q values (Q being the magnitude of the neutron wave-vector) in the range from 0.2 $\text{Å}^{-1} \leq\ Q\ \leq 2.00\ \text{Å}^{-1}$, the nature of water dynamics can be investigated at a molecular level.

The experimentally determined double differential scattering cross section is directly related to the self-dynamic structure factor, $S_H(Q,\omega)$, which is the Fourier transform of the self intermediate scattering function (ISF), $F_H(Q,t)$, of the hydrogen atom in a water molecule. These connections facilitate the interpretation of the scattering data and allow a direct comparison with theory and with the data from MD simulations.

Here we present a systematic investigation of temperature and pressure dependences of dynamics of water inside nanoporous silica materials. The temperature range covers from room temperature down to deeply supercooled states, and the pressure ranges from ambient to 2.4 $k$bar. QENS data collected are analyzed according to a single consistent model RCM, which is valid for bulk as well as confined water as was shown by MD simulations [21, 22, 23, 24, 25, 26, 27].

Chapter 2

Experimental and Computer Simulation Methods

2.1 Sample Description

Different mesoporous matrices, e.g. Vycor [17, 29, 41, 42], GelSil [43, 44], clay [45, 46], MCM-41 [47, 48, 49, 50], have been used as confining media. Among the different nanoporous silica matrices, the relatively recently discovered MCM represents an interesting opportunity for studying water in confinement. For example, in comparison with Vycor glass, these molecular sieves have smaller pores with a narrower size distribution.

The MCM samples allow us to study dynamical effects of different pore morphologies and the small dimensions of these pores allow us to investigate temperatures below the homogeneous nucleation temperature.

2.1.1 Sample preparation

To synthesize the MCM samples, zeolite seeds were prepared by mixing $NaAlO_2$ (Riedel-de Haen), NaOH (Shimakyu's Pure Chemicals, Japan) fumed silica (Sigma), tetraethyl ammonium hydroxide (TEAOH) aqueous solution (20 %) (Acros), and water under stirring for 2 to 5 h, then placing the solution in an autoclave at 100 °C for

18 h. MCM-48-S[1] [51] was synthesized by reacting zeolite seeds with cetyltrimethylammonium bromide solution (CTAB, Acros) at 150 °C for 6 h to 24 h. Samples were then collected by filtration, washed with water, dried at 100 °C in an oven for 6 h, and calcined at 580 °C for 6 h. To obtain MCM-41-S [52] we follow a similar method for synthesizing MCM-48-S. Using the short chain cationic surfactant dodecyltrimethylammonium, C_{12}TMAB, as templates and adding β-type zeolite seeds as silica source [52], we obtain MCM-41-S with smaller pore sizes and stronger silica walls than the traditional MCM-41[2]. In both cases the molar ratios of the reactants NaAlO2 : SiO2 : NaOH: TEAOH: C_{16}TMAB: H_2O were 1:37-67:1.5-9:11-22:18.3:3000-3500.

Micellar templated mesoporous silica matrix MCM-48-S was well ordered structure with 3-D bicontinous morphology, whereas MCM-41-S has 1-D cylindrical pores arranged in 2-D hexagonal arrays, which was determined by x-ray diffraction (XRD) method and shown in Fig. 2-1. Pore diameters are $1 \sim 3$ nm obtained by nitrogen adsorption technique. Putting the calcined samples into the diskette that was full of water vapor by pumping the saturated NaCl solution will make them full-hydrated in $2 \sim 3$ days. Then, the hydration levels of water-loaded samples are around 20-60 % by determination of thermogravimetric analysis (TGA).

2.1.2 Sample characterization

The samples have been characterized using XRD (Scintag X1 diffractometer using Cu Kα, $\lambda = 0.154$ nm), transmission electron microscopy (TEM), thermogravimetric analysis (TGA) (NETZSCH TG-209), and differential scanning calorimetry (DSC) (TA Instrument 5100 control system and a LT-Modulate DSC 2920). N_2 adsorption-desorption isotherms have been measured as well (Micromeritics ASAP 2010 sorptometer at 77 K).

[1] S denotes seed.

[2] The MCM-41-S materials are able to withstand prolonged ($\geq$ 1 month) exposure to water at room temperature without structural decay.

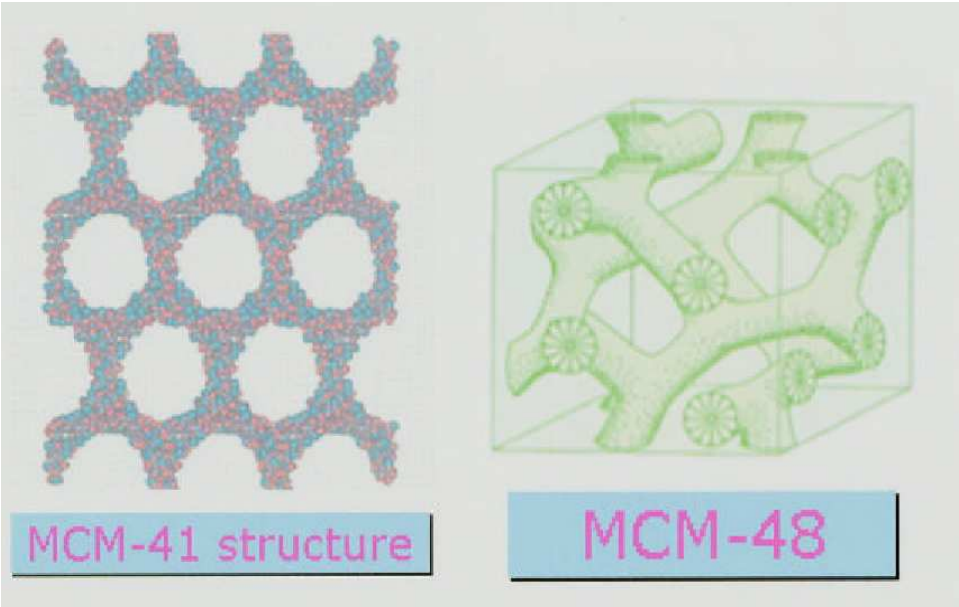

Figure 2-1: Microscopic structures of MCM-41-S and MCM-48-S.

XRD spectra show that the MCM-48-S was well ordered with cubic (Ia3d) symmetry, whereas the MCM-41-S had hexagonal (P6mm) symmetry, as shown in Fig. 2-2. Both samples exhibit high hydrothermal stability. BET surface area, pore size[3] and pore volume were determined using the nitrogen adsorption-desorption technique. The obtained values are reported in Table 2.1. The wall thickness of the MCM-48-S sample is about 10 Å, as calculated using the Schumacher's method [53].

The XRD figure (Fig. 2-2) shows the well-order of the samples,which is explained by the sharp peaks. The (1 0 0) peak (the highest peak) is related to the d-spacing. If the pore size of the sample is smaller, the (1 0 0) peak will show in a higher angle. According to the rule : $2d \sin(\theta) = n \times \lambda$, $\lambda = 1.54$ is a constant. So $d = 1/(\sin\theta)$. And since the samples do not show a peak in the high angle region, it means we have just one phase (pure phase).

[3]Pore size is determined by the capillary condensation in the standard Barrett-Joyner-Halenda (BJH) method in nitrogen adsorption experiment (at 77 K). Because of the uncertainty in estimating the thickness of surface immobile layer, the pore size is a nominal estimation.

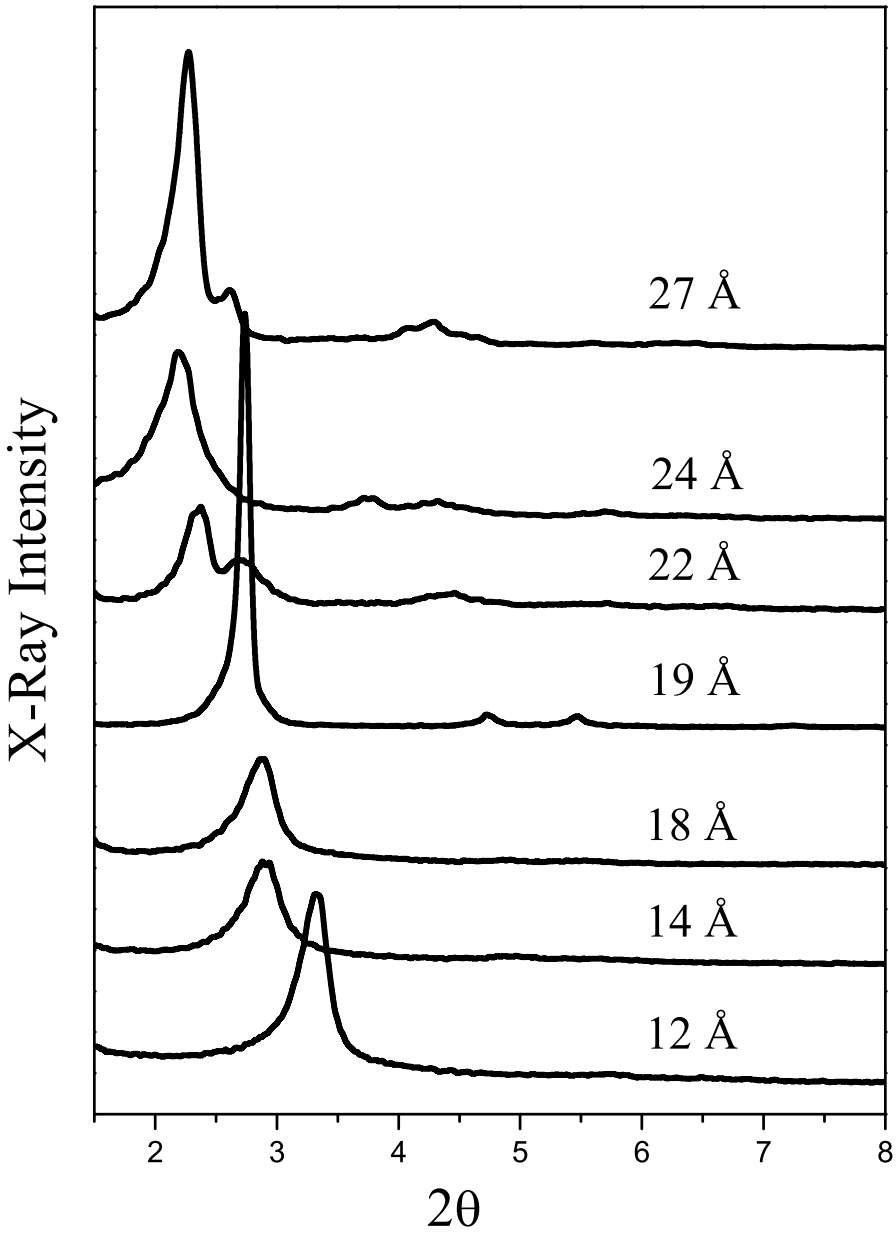

Figure 2-2: X-ray diffraction of MCM-48-S and MCM-41-S.

Table 2.1: Parameters characterizing the structural properties of the investigated samples.

Samples	Surface area	Pore size	Pore volume	Hydration level	T_m
Mac-48-S-27	1312 (m^2/g)	27.0 (Å)	0.97 (cm^3/g)	48 (wt%)	248 (K)
Mac-41-S-24	1358 (m^2/g)	24.0 (Å)	1.38 (cm^3/g)	50 (wt%)	220 (K)
Mac-41-S-22	1156 (m^2/g)	22.0 (Å)	1.08 (cm^3/g)	51 (wt%)	202 (K)
Mac-41-S-19	1170 (m^2/g)	19.0 (Å)	0.76 (cm^3/g)	49 (wt%)	174 (K)
Mac-41-S-18	1384 (m^2/g)	18.0 (Å)	0.67 (cm^3/g)	55 (wt%)	165 (K)
Mac-41-S-14	726 (m^2/g)	14.0 (Å)	0.41 (cm^3/g)	50 (wt%)	129 (K)
Mac-41-S-12	1018 (m^2/g)	12.0 (Å)	0.65 (cm^3/g)	48 (wt%)	110 (K)
Mac-41-S-10	875 (m^2/g)	10.0 (Å)	0.49 (cm^3/g)	40 (wt%)	92 (K)

In the later part of this thesis, we only choose the silica with a pore diameter of 14 Å to perform the pressure experiments because for the fully hydrated sample the DSC data shows no freezing peak down to 160 K. According to the Gibbs-Thomson equation [54], the melting point of small crystal is inversely proportional to the crystal size, which, in this case, is equal to the pore size of the material. The melting/freezing behavior of water in the samples has been checked by DSC measurements (Fig. 2-3). Thus, for example, the MCM-48-S-27 sample has a higher melting point than the MCM-41-S-22 sample. The estimated melting points are $T_m = 248$ and 220 K, for water in the MCM-48-S-27 and MCM-41-S-22 matrices, respectively. The calculated T_m values are reported in the last column of Table 2.1.

2.2 Experimental Method – Quasi-Elastic Neutron Scattering (QENS)

High-resolution QENS spectroscopy method is used to determine the temperature and pressure dependences of the average translational relaxation time, $\langle \tau_T \rangle$, for the confined water. Because neutrons can easily penetrate the thick-wall high-pressure cell and because it is predominantly scattered by hydrogen atoms in water, rather

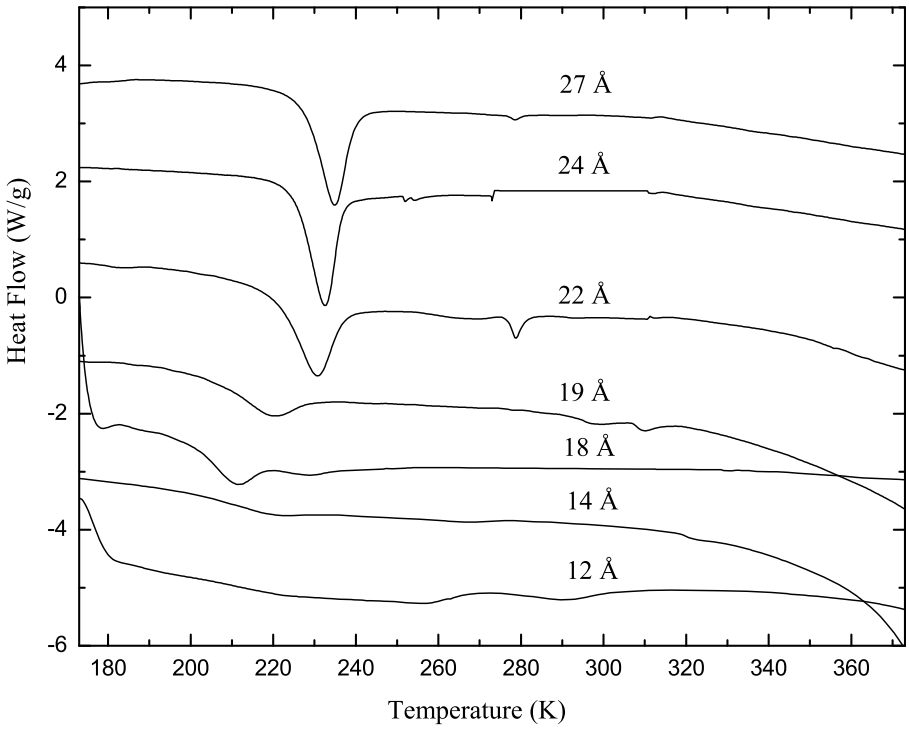

Figure 2-3: DSC curves for the water-filled MCM-48-S and MCM-41-S samples determined at the heating rate 10 °C/min after cooling to -100 °C.

than by the matrices containing it, incoherent QENS is an appropriate tool for our study. Using three separate high-resolution QENS spectrometers, we are able to measure the translational relaxation time from 0.2 *ps* to 10,000 *ps* over the temperature and pressure range. The experiments were performed at the High-Flux Backscattering (HFBS), the Disc-Chopper Time-of-Flight (DCS) and the Fermi-Chopper (FCS) spectrometers in the NIST Center for Neutron Research (NIST NCNR). The three spectrometers used to measure the spectra have widely different dynamic ranges (for the chosen experimental setup). HFBS has an energy resolution of 0.8 μeV and a dynamic range of ± 11 μeV [55]; DCS has an energy resolution of 20 μeV and a dynamic range of ± 0.5 meV [56]; and FCS has an energy resolution of 60 μeV and a dynamic range of ± 1.5 meV. We purposely selected these three experimental tools in order to be able to extract the broad range of relaxation times from the measured spectra.

In the high-resolution QENS experiments at ambient pressure, a hydrated powder of MCM-41-S or MCM-48-S was evenly spread to form a rectangular slab sample 0.5 mm thick, such that multiple-scattering corrections should not be necessary (transmission ≥ 95 %). However, for a high-pressure experiment, the same high pressure system, including specially designed aluminium pressure cell, was used on both HFBS and DCS instruments. Helium gas, the pressure-supplying medium, fills the whole sample cell, and applies pressure to the fully hydrated sample. The experiment at each pressure was done with a series of temperatures, covering both below and above the proposed Fragile-to-Strong transition temperatures. Altogether, more than 1100 spectra were collected, spanning a series of ambient pressure experiments for water hydrated in MCM with different pore sizes and MCM-41-S-14 under 10 pressures: ambient, 100, 200, 400, 800, 1200, 1400, 1600, 2000, and 2400 bars.

2.3 Computer Simulation Method – Molecular Dynamics (MD)

We perform MD simulations of 216 water molecules at temperatures T = 284.5, 263.0, 250.0, 225.0, 220.0 and 215.0 K, interacting via the extended-simple-point-charge (SPC/E) pair potential [57]. This is a more suitable method to test out our model of decoupling approximation and the rotational correlation functions than using real neutron scattering data, since MD data do not have the complication of the resolution effect as real experimental data. We carried out an extensive simulation, in an NVE (constant number of molecules N, constant volume V, and constant energy E) ensemble with 216 water molecules contained in a cubic box of an edge 18.65 Å. The effective potential used is the extended-simple-point-charge model SPC/E. This potential treats a single water molecule as a rigid set of point masses with an OH distance of 0.1 nm and an HOH angle equal to the tetrahedral angle 109.47°. The point charges are placed on the atoms and their magnitudes are $q_H = 0.4238e$ and $q_O = -2q_H = -0.8476e$. Only the oxygen atoms in different molecules interact among themselves via a Lennard-Jones potential, with the parameters $\sigma = 0.31656$ nm and $\epsilon = 0.64857$ kJ/Mol. The interaction between pairs of molecules is calculated explicitly when their separation is less than a cutoff distance r_c of 2.5σ. The contribution due to Coulomb interactions beyond r_c is calculated using the reaction-field method, as described by Steinhauser [58]. Also, the contribution of Lennard-Jones interactions between pairs separated by more than r_c is included in the evaluation of thermodynamic properties by assuming a uniform density beyond r_c. A heat bath [59] has been used to allow for heat exchange when changing temperature of the system. After the system has been equilibrated, the heat bath is then removed. In our simulations, periodic boundary conditions are used. The time step for the integration of the molecular trajectories is 1 fs. Simulations at low T were started from equilibrated configurations at higher T. Equilibration was monitored via the time dependence of the potential energy. In all cases the equilibration time t_{eq} was longer than the time needed to enter the diffusive regime. We note that for SPC/E model of water, the

Table 2.2: Simulated state points

T(k)	ρ_s(g/cm^3)	E(kJ/mol)	P(MPa)	D(10^{-5}cm^2/s)
284.5	0.984	-48.1	-73 ± 11	$(1.3 \pm 0.1) \times 10^0$
263.0	0.985	-49.4	-70 ± 12	$(7.5 \pm 0.6) \times 10^0$
250.0	0.986	-50.0	-76 ± 12	$(5.2 \pm 0.5) \times 10^{-1}$
225.0	0.984	-52.6	-75 ± 15	$(4.4 \pm 0.4) \times 10^{-2}$
220.0	0.984	-53.1	-72 ± 16	$(6.2 \pm 0.3) \times 10^{-3}$
215.0	0.984	-53.7	-75 ± 18	$(1.2 \pm 0.1) \times 10^{-3}$

density maximum occurs at about 250 K, which corresponds to 277 K in the real water. For the lower temperatures, 225 K to 210 K, we recorded water trajectories for more than 1 ns. And for the other temperatures we recorded for 0.1 ns. Further detailed thermodynamic parameters of the simulations are given in Refs. [24] and [57].

In the investigated Q-range, the vibrational contribution drops out of consideration (explained later). Because of the above mentioned simplification, in a molecular dynamics simulation the QENS spectra can be obtained taking water to be effectively a rigid molecule using, for example, the SPC/E model potential.

The SPC/E potential has been explicitly parameterized to reproduce the experimental value of the self-diffusion constant at ambient temperature and at a density of 1 g/cm^3[59]. Densities in our simulation have been chosen on the basis of trial and error in preliminary runs. The corresponding pressures for the chosen final densities are reported in Table 2.2, and it has been well described in [24]. The complete SPC/E MD simulation code is attached in Appendix B.

Chapter 3

Relaxing-Cage Model (RCM)

3.1 Introduction

We use ideas from Mode-Coupling Theory (MCT) of supercooled liquids to formulate the Relaxing-Cage Model (RCM) [21]. The cage effect in the liquid state, which can be pictured as a transient trapping of molecules as a result of lowering the temperature or on increasing the density, is a main idea in MCT [60, 61]. Microscopic density fluctuations of disordered high temperature and low density fluids usually relax rapidly in a time scale of a few picoseconds. Then, upon lowering the temperature below the freezing point or increasing the density of the liquid by applying a pressure, a rapid increase in the local order surrounding a particle, called a cage, leads to a substantial increase of the local structural relaxation time. A trapped particle in a cage, in the dense or supercooled liquid regime, can only migrate through rearrangement of a large number of particles surrounding it. Therefore, there is a strong coupling between the single particle motion and the density fluctuations of the fluid. According to MCT, the long time cage structural relaxation behavior is completely determined by the equilibrium structure factor $S(Q)$ of the liquid. It predicts that at the singular temperature, T_s, the structural relaxation time becomes infinity and the supercooled liquid shows a phenomenon of structural arrest. On approaching T_s from above, there is a larger and larger separation between the time scales describing the rattling motion of a particle in the cage and the eventual structural relaxation time

of the cage. Numerically, various model systems, such as the hard sphere system [62] or a mixed Lennard-Jones system [63], have shown this prediction and that the time evolution of the structural relaxation (called the α relaxation) is well approximated by a stretched exponential decay with a system dependent stretch exponent.

3.2 Theoretical Model

Upon supercooling, water undergoes an expansion or lowering of density. On lowering the temperature below the freezing point, water develops a tendency to form a hydrogen-bonded, tetrahedrally coordinated first and second neighbor shell around a given molecule. Compared with five or six neighbor configurations which are known to be present with higher probability at higher temperatures, this configuration is a more open structure, so that the structural relaxation time of water increases rapidly upon supercooling since the tetrahedrally coordinated hydrogen-bonded structure, shown in Fig. 3-1, is an inherently more stable structure locally and has a longer lifetime. At short times, less than 0.05 ps, the water molecule performs harmonic vibrations and librations inside the cage; at long times, longer than 1.0 ps, the cage eventually relaxes and the trapped particle can migrate through the rearrangement of a large number of particles surrounding it. Thus, the center of mass motion of a supercooled water molecule can be considered as a compounded motion of a short-time in-cage vibrations and a long-time cage relaxation, having two widely separated time scales. This is so-called Relaxing-Cage Model. To analyze the translational and rotational dynamics of water at supercooled temperature, we have developed the RCM in the past few years. This model has been tested with MD simulations of SPC/E water [21, 22], and has been used to analyze QENS data [64, 65, 66].

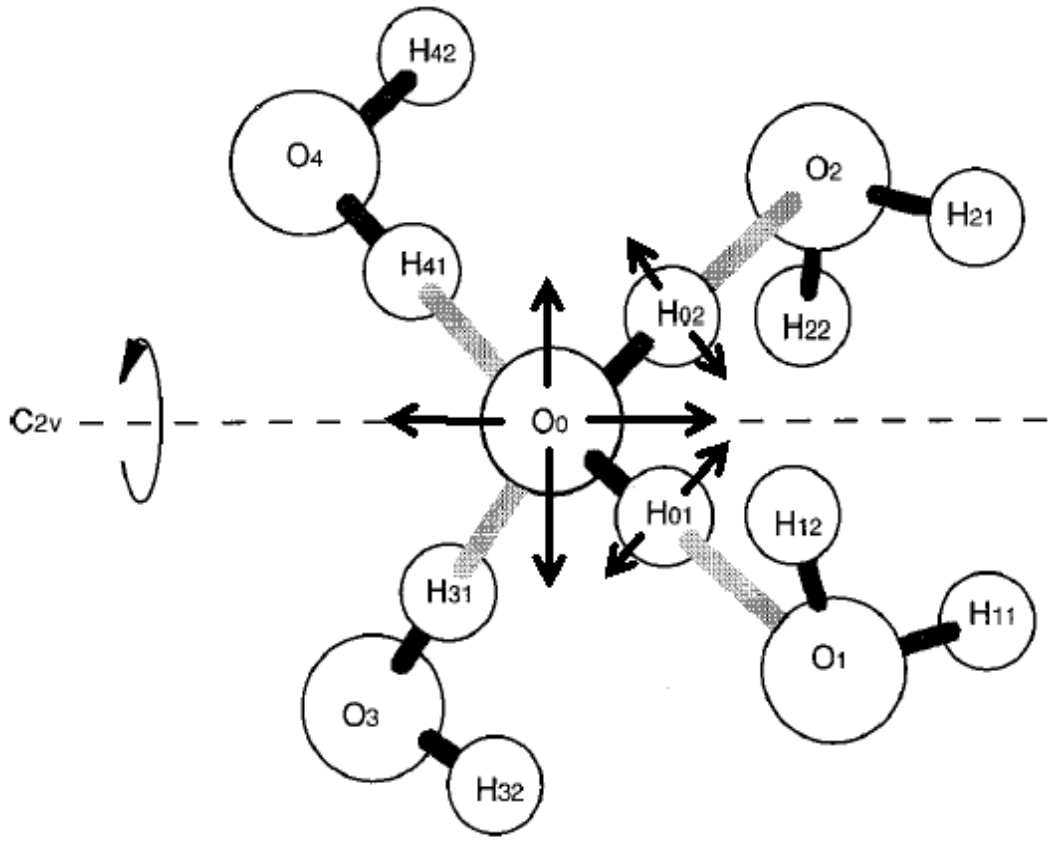

Figure 3-1: A schematic diagram for the hydrogen-bonded, tetrahedrally coordinated nearest neighbor cage in supercooled water.

3.2.1 Dynamic structure factor

Since the incoherent scattering cross-section of hydrogen is roughly twenty times larger than the total scattering cross-section of oxygen, silicon, and aluminum in the porous matrices, we may only take into account the contribution from the hydrogen atoms in the double differential scattering cross-section of water and deal with the self dynamic structure factor of the hydrogen atoms in the water molecules. In a QENS experiment, we can measure double differential scattering cross-section $d^2\sigma_H/d\Omega d\omega$, where σ_H, is the incoherent scattering cross-section of a hydrogen atom, $d\Omega$ is the differential solid angle into which the neutron is scattered and $E = \hbar\omega$ is the energy transferred by the neutron to the sample. We have a well-known relation:

$$\frac{d^2\sigma_H}{d\Omega d\omega} = 2N\frac{\sigma_H}{4\pi}\frac{k_f}{k_i}S_H(Q,\omega) \tag{3.1}$$

where N is the number of water molecules in the sample, k_i and k_f are, respectively, the wave number of the incident and scattered neutrons, and $S_H(Q,\omega)$ is the self-dynamic structure factor. Since N, σ_H, k_i and k_f are all known quantities in a QENS experiment, $S_H(Q,\omega)$ can be straightforwardly extracted from the double differential scattering cross-section.

In van Hove theory of neutron scattering [67], $S_H(Q,\omega)$ is given in terms of the Fourier transform of the intermediate scattering function (ISF) of the hydrogen atom, $F_H(Q,t)$, according to the equation:

$$S_H(Q,\omega) = \frac{1}{2\pi}\int_{-\infty}^{\infty} dt e^{i\omega t}F_H(Q,t). \tag{3.2}$$

We can then see that $F_H(Q,t)$ is the primary quantity of theoretical interest related to experiments. It can be calculated by a model, such as RCM, and molecular dynamics simulation of SPC/E model of water.

3.2.2 Decoupling approximation

The dynamics of a hydrogen atom is composed of three components: the vibrational motion of the atom around its equilibrium position, the rotational motion of the atom around C. M.[1], and the translational motion of C. M.. The decoupling approximation [68] has been generally assumed in the analysis of QENS data of water. In this approximation, the ISF of the hydrogen atoms is written as the product of the vibrational ISF, $F_V(Q,t)$, rotational ISF, $F_R(Q,t)$, and translational ISF, $F_T(Q,t)$:

$$F_H(Q,t) = F_T(Q,t) \cdot F_R(Q,t) \cdot F_V(Q,t). \tag{3.3}$$

The vibrational contribution, or the inelastic contribution, can be well approximated by a Debye Waller factor [69], $\exp\left[-\frac{1}{3}\langle u^2\rangle Q^2\right]$. This is because we are concerned only with analysis of neutron spectra in the quasi-elastic region ($0 < E < 3000$ μeV), which is equivalent to a time-scale of picosecond or longer in the ISF. $\langle u^2\rangle$ is the mean square vibrational amplitude of the hydrogen atom around its equilibrium position. Since O-H distance in a water molecule is about 1 Å, $\sqrt{\langle u^2\rangle} \leq 0.1$ Å. In the investigated Q range ($Q < 2$ Å), the vibrational Debye Waller factor is essentially unity. This also implies the validity of SPC/E model in simulating ISF by assuming a rigid water molecule. As the consequence, the ISF of the hydrogen atoms can be expressed as the product of the rotational and translational ISFs,

$$F_H(Q,t) = F_T(Q,t) \cdot F_R(Q,t) \tag{3.4}$$

3.2.3 The validity of the decoupling approximation

We start to discuss the validity of the decoupling approximation, Eq. 3.4, by defining a new function, $F_{CON}(Q,t)$. From the definition of intermediate scattering function, $F_H(Q,t) = \left\langle e^{-i\vec{Q}\cdot(\overrightarrow{r}(t)-\overrightarrow{r}(0))}\right\rangle$, where $\overrightarrow{r}(t)$ if the position of the hydrogen atom at time t. Since $\overrightarrow{r}(t) = \overrightarrow{R}(t) + \overrightarrow{b}(t)$, where $\overrightarrow{b}(t)$ denotes a vector from the center of mass to the hydrogen atom and $\overrightarrow{R}(t)$ denotes the position of the center of mass, we

[1] C. M. stands for the center of mass of the water molecule

can rewrite $F_H(Q,t)$ as the product of four factors,

$$F_H\left(Q,t\right) = \left\langle e^{-i\vec{Q}\cdot\overrightarrow{R}(0)} e^{-i\vec{Q}\cdot\vec{b}(0)} e^{i\vec{Q}\cdot\overrightarrow{R}(t)} e^{i\vec{Q}\cdot\vec{b}(t)} \right\rangle . \tag{3.5}$$

When dealing with a correlation function that is a product of four terms, each one with a (Q,t) dependence, it is generally possible to rewrite it as the sum of all the possible binary factorizations of its terms plus another irreducible term, which we now call the connected intermediate scattering function $F_{CON}\left(Q,t\right)$,

$$\begin{aligned} F_H\left(Q,t\right) &= \left\langle e^{-i\vec{Q}\cdot\overrightarrow{R}(0)} e^{i\vec{Q}\cdot\overrightarrow{R}(t)} \right\rangle \times \left\langle e^{-i\vec{Q}\cdot\vec{b}(0)} e^{i\vec{Q}\cdot\vec{b}(t)} \right\rangle \\ &\quad + \left\langle e^{-i\vec{Q}\cdot\overrightarrow{R}(0)} e^{i\vec{Q}\cdot\vec{b}(t)} \right\rangle \times \left\langle e^{i\vec{Q}\cdot\overrightarrow{R}(t)} e^{-i\vec{Q}\cdot\vec{b}(0)} \right\rangle + F_{CON}\left(Q,t\right). \end{aligned} \tag{3.6}$$

The time dependence of $\overrightarrow{b}(t)$ is independent of the choice of the reference system. In the reference system defined by the molecular center of mass $\overrightarrow{R}(t)$, all mixed correlation functions vanish. Therefore, the contributions, arising from all the terms composed of products of $\vec{R}$ and $\vec{b}$ variables at an arbitrary time, are zero on average. Generally speaking, $F_{CON}\left(Q,t\right)$ is different from zero and contains the contribution coming from the four factors coupled together in the correlation function. So that we can get the following relation,

$$F_H\left(Q,t\right) = F_T\left(Q,t\right) F_R\left(Q,t\right) + F_{CON}\left(Q,t\right) \tag{3.7}$$

where $F_{CON}\left(Q,t\right)$ describes the strength of the coupling between translational and rotational motions as a function of Q and t, as observed by QENS. Even though the rotational and translational motions of a water molecule are strongly coupled at all time [22, 25], MD simulations of SPC/E water at supercooled temperature have shown that the decoupling approximation is good to a few percent.

In the graphs of Fig. 3-2 we show in a semi-logarithmic scale the following four

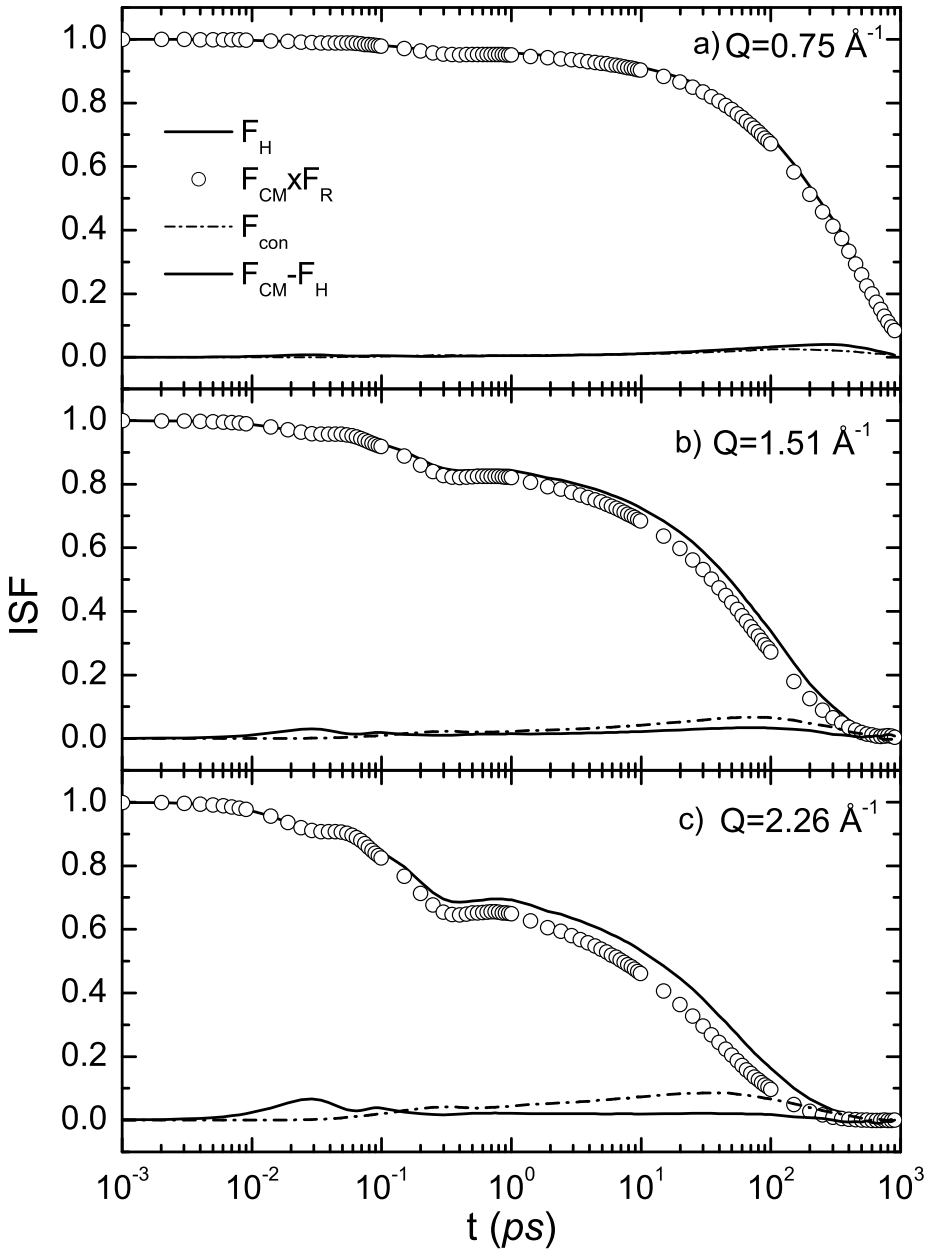

Figure 3-2: The intermediate scattering functions(ISF) at three Q values (0.75 Å^{-1}, 1.51 Å^{-1}, and 2.26 Å^{-1}) and at $T = 225$ K, as a function of time in logarithmic scale.

quantities: $F_H(Q,t)$, $F_{CM}(Q,t) \times F_R(Q,t)$, $F_{CON}(Q,t)$ and $F_{CM}(Q,t) - F_H(Q,t)$. These functions are shown for a temperature 225 K at three Q values. These Q values are also quite close to the maximum and the minimum Q value that can be probed by a typical QENS experiment. The top solid lines represent $F_H(Q,t)$; the open circles , $F_{CM}(Q,t) \times F_R(Q,t)$; the dash-dot line, the connected part of the correlation function, $F_{CON}(Q,t)$ and the thick solid line, the difference, $F_{CM}(Q,t) - F_H(Q,t)$. It is to be noted that at low Q, the decoupling approximation is good but at high Q, the approximation progressively becomes poorer at long time but the deviation never exceeds 0.09. However it is also noticeable that at long time ($t > 1$ ps) F_H nearly coincides with F_{CM} .We see that $F_H(Q,t)$ has the same short-time features as $F_{CM}(Q,t) \times F_R(Q,t)$ but the same long-time feature as $F_{CM}(Q,t)$, so that $F_{CON}(Q,t)$ is very small at time smaller than 1 ps but becomes non-negligible for long time. On the contrary $F_{CM}(Q,t) - F_H(Q,t)$ is negligible at time longer than 1 ps but large at short time. Both $F_{CON}(Q,t)$ and $F_{CM}(Q,t) - F_H(Q,t)$ increase substantially with the increasing of Q value, but never reach 0.09 in magnitude.

In the graphs of Fig. 3-3, we showed that the coupling of rotational and translational motions is in general non-negligible for high-Q values. Also note as the Fourier transform of the fit to the intermediate scattering functions of the center of mass and the hydrogen atoms and the direct Fourier transform of the connected correlation contribution. The solid lines represent $S_H(Q,\omega)$; the dash lines, $S_{CM}(Q,\omega)$; the dash-dot line, and the connected part of the structure factor, $S_{CON}(Q,\omega)$. It is to be noted that only at low frequency, $S_{CM}(Q,\omega)$ is different from $S_H(Q,\omega)$ by showing a higher peak. This difference increases as Q gets bigger, but never exceeds 0.09. In the frequency space, the difference between the center of mass and the hydrogen is not as big as the contribution from $F_{CON}(Q,t)$.

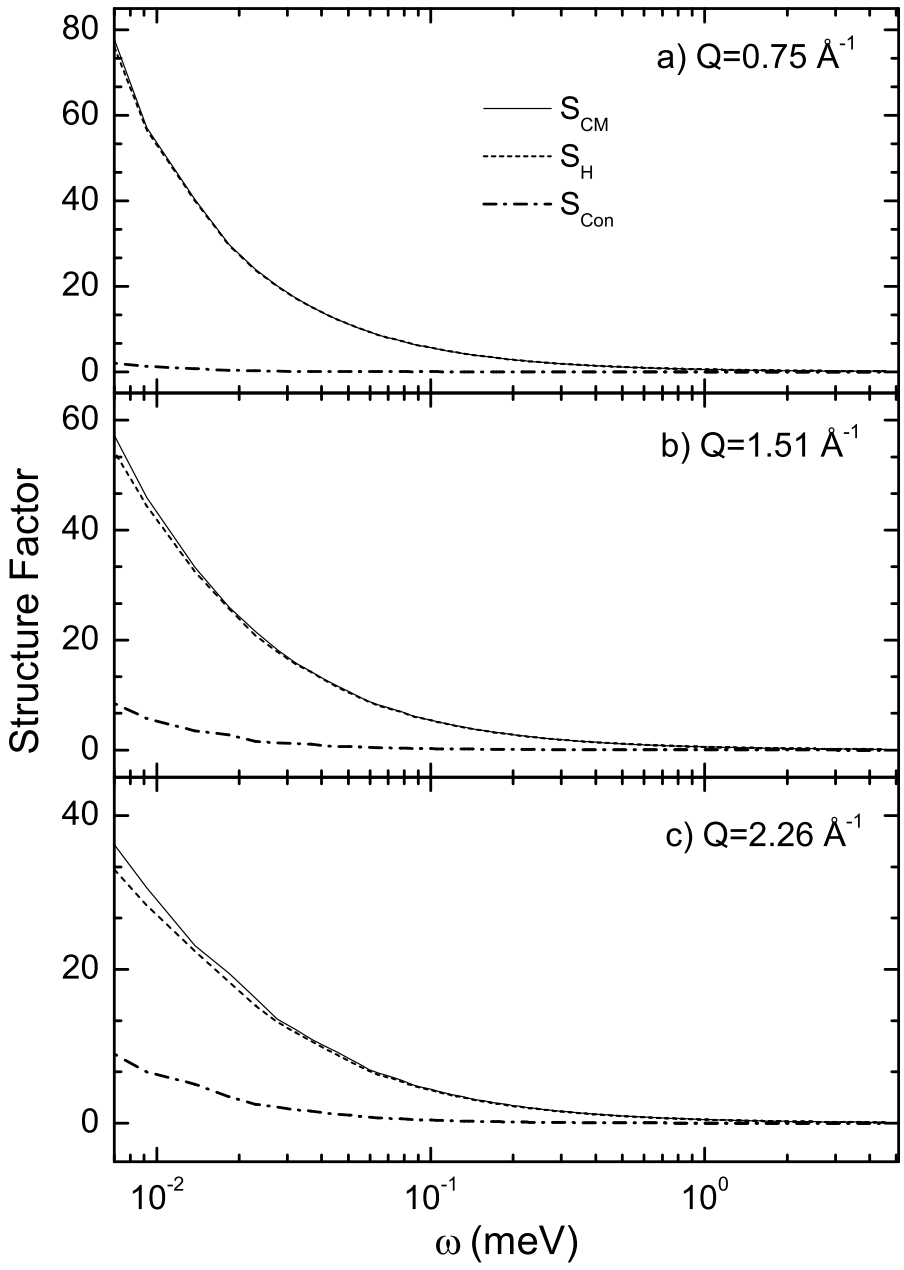

Figure 3-3: The dynamic structure factor at three Q values (0.75 Å^{-1}, 1.51 Å^{-1}, and 2.26 Å^{-1}) and at $T = 225$ K, as a function of frequency in logarithmic scale.

3.2.4 Theory for the translational intermediate scattering function

Having established the validity of the decoupling approximation, Eq. 3.4, we now discuss how to get the translational and the rotational intermediate scattering functions separately. For translational ISF, the Relaxing Cage picture gives us an idea to express $F_T(Q,t)$ in terms of the product of the short-time dynamics and a long-time decay of the ISF. This is because the time scale for the in-cage vibrational motion and the long-time relaxation of the cage itself are well separated in the supercooled water. We first discuss about the short-time part of the ISF.

The RCM assumes that the translational short-time dynamics of the trapped water molecule can be treated approximately as the motion of the center of mass in an isotropic harmonic potential well, provided by the mean field of its neighbors. Then, by using the so-called Bloch identity, which is valid for a system with a simple harmonic oscillator Hamiltonian, we connect the short time part of the translational ISF to the center of mass velocity auto-correlation function, $\langle \vec{v}_{CM}(t) \cdot \vec{v}_{CM}(0) \rangle$:

$$F_T^s(Q,t) = \exp\left\{ -Q^2 \left[\int_0^t (t-\tau) \langle \vec{v}_{CM}(0) \vec{v}_{CM}(\tau) \rangle d\tau \right] \right\} \tag{3.8}$$

The density of states, $Z(\omega)$, is another key parameter and it has translational and rotational parts. The translational part of the density of states, $Z_T(\omega)$, which can be measured by inelastic neutron scattering experiments, is the Fourier transform of the center of mass velocity auto-correlation function:

$$Z_T(\omega) = \frac{1}{2\pi} \int_{-\infty}^{\infty} e^{i\omega t} \langle \vec{v}_{CM}(0) \cdot \vec{v}_{CM}(\tau) \rangle / \langle v_{CM}^2 \rangle dt \tag{3.9}$$

where M is the mass of the particle, and $\langle v_{CM}^2 \rangle = \langle v_x^2 \rangle + \langle v_y^2 \rangle + \langle v_z^2 \rangle = 3v_0^2 = 3k_BT/M$ is the average center of mass square velocity.

Both MD and experiment results show that the translational harmonic motion of a water molecule in the cage gives rise to two characteristic peaks in $Z_T(\omega)$ (or

$Z_{CM}(\omega)$) at about 10 and 30 meV, respectively [41]. Therefore, the following Gaussian functional form has been suggested for the translational part of the density of states:

$$Z_T(\omega) = 2(1-C)\frac{\omega^2}{\omega_1^2\sqrt{2\pi\omega_1^2}}\exp\left[-\frac{\omega^2}{2\omega_1^2}\right] + 2C\frac{\omega^2}{\omega_2^2\sqrt{2\pi\omega_2^2}}\exp\left[-\frac{\omega^2}{2\omega_2^2}\right] \qquad (3.10)$$

where $\sqrt{2}\omega_1$ and $\sqrt{2}\omega_2$ are the frequencies of the two characteristic peaks in $Z_T(\omega)$, and C is the relative strength of the two peaks. The fit of MD results using Eq. 3.10 gives $C = 0.44$, $\omega_1 = 10.8$ THz, and $\omega_2 = 42.0$ THz.

We get an expression for $F_T^s(Q,t)$, using Eqs. 3.8-3.10:

$$F_T^s(Q,t) = \exp\left\{-Q^2v_0^2\left[\frac{1-C}{\omega_1^2}\left(1-e^{-\omega_1^2t^2/2}\right) + \frac{C}{\omega_2^2}\left(1-e^{-\omega_2^2t^2/2}\right)\right]\right\} \qquad (3.11)$$

It should be noted that Eq. 3.11 is the short-time behavior of the translational ISF; it starts from unity at $t = 0$ and decays rapidly; and in the long-time limit (longer than 1 ps), $F_T^s(Q,t)$ decays to a plateau given by an incoherent Debye-Waller factor $A(Q)$:

$$A(Q) = \exp\left\{-Q^2v_0^2\left[\frac{1-C}{\omega_1^2} + \frac{C}{\omega_2^2}\right]\right\} = \exp\left[-Q^2a^2/3\right] \qquad (3.12)$$

where a is the root mean-square vibrational amplitude of the water molecules in the cage, in which the particle is constrained during its short-time movements. Both MD and QENS experiments gave the value, $a \approx 0.5$ Å, in the supercooled region. a is fairly temperature independent [23].

According to the Mode-Coupling Theory (MCT), the cage relaxation at long-time can be described by the α-relaxation model, with a stretched exponential time decay. This α-relaxation model is described by two parameters, the structural relaxation time τ_T, which is Q dependent, and a stretch exponent β, also slightly Q dependent. Therefore, the complete time dependence of translational ISF can be written as:

$$F_T(Q,t) = F_T^s(Q,t)\exp\left[-(t/\tau_T)^\beta\right]. \tag{3.13}$$

Previously, Chen et al [21] has shown that τ_T has a power-law like dependence on Q with a pre-factor τ_0 and a power-law exponent γ,

$$\tau_T = \tau_0(aQ)^{-\gamma}. \tag{3.14}$$

We call τ_0 the average temperature-dependent translational relaxation time and γ the exponent for the Q-dependence of τ_T. We therefore focus our discussions on τ_0 and γ instead of τ_T. MD results show that the exponent γ has a slight Q-dependence while approaching 2 in the limit $Q \to 0$ and remains constant at higher Q values. The stretch exponent, β, is slightly Q dependent as well while approaching 1 at high temperature and in the limit $Q \to 0$. These limits lead to the normal diffusion process at low Q values, $F_T(Q,t) \approx \exp[-DQ^2t]$, where D is the self-diffusion coefficient. Whereas our experiment is out of this low Q limit, both β and γ may be considered Q-independent [64, 65].

3.2.5 Theory for the rotational intermediate scattering function

As far as the rotational ISF is concerned, we start from an exact expansion of it generated by Sears [70]. Like we defined earlier, $\vec{b}(t)$ denotes a vector from the center of mass to the hydrogen atom. The rotational ISF could be then expressed by this vector, as the water molecule rotates around the center of mass,

$$F_R(Q,t) \equiv \left\langle e^{-i\vec{Q}\cdot\vec{b}(0)}e^{i\vec{Q}\cdot\vec{b}(t)}\right\rangle = j_0^2(Qb) + \sum_{\ell=1}^{\infty}(2\ell+1)j_\ell^2(Qb)C_\ell(t) \tag{3.15}$$

where $j_\ell(x)$ stands for the ℓ-th order spherical Bessel function; $C_\ell(t)$, the ℓ-th order rotational correlation function and $b = 0.98$ Å, the approximate length of the O-H bond in a water molecule. For a typical Q-range encountered in QENS experiments,

generally $Q < 2.5$ Å^{-1}, this expansion is very useful. The advantage of using this expansion is that the Q -dependence of the rotational ISF is exactly given and one needs to make a model for a few lower order rotational correlation functions which are Q-independent quantities. In this case, the expansion needs to be carried out to at most $\ell = 3$ term. In this paper, we shall make a model explicitly for the function $C_1(t)$ and shall generate the other higher-order rotational correlation functions approximately using the maximum entropy method of Berne et al [71].

The ℓ-th order rotational correlation function is defined as

$$C_\ell(t) = \langle P_\ell(\cos\theta(t))\rangle \tag{3.16}$$

where $\theta(t)$ is the angle between the vector $\vec{b}(0)$ and $\vec{b}(t)$. To calculate the statistical average, we start by considering the short time behavior of $C_1(t)$. At a given instant, call $t = 0$, a typical hydrogen atom is hydrogen-bonded to its nearest neighbor oxygen atom. Then, the short-time dynamics of the rotation of the hydrogen, $\vec{b}(t)$, around the center of mass must be well described by a harmonic motion of the angle $\theta(t)$, that is to say

$$\ddot{\theta}(t) + \omega^2\theta(t) = 0. \tag{3.17}$$

Then the distribution function of $\theta(t)$ is gaussian and it follows the Bloch theorem [72]:

$$\left\langle e^{\alpha\theta}\right\rangle = \exp\left[\frac{1}{2}\left\langle(\alpha\theta)^2\right\rangle\right]. \tag{3.18}$$

Known that

$$P_1(\cos\theta(t)) = \cos\theta(t) = \frac{e^{i\theta} + e^{-i\theta}}{2}, \tag{3.19}$$

one can then derive the following results:

$$C_1^s(t) = \langle\cos\theta(t)\rangle = \left\langle\frac{e^{i\theta} + e^{-i\theta}}{2}\right\rangle = \exp\left[-\frac{1}{2}\left\langle\theta^2(t)\right\rangle\right]. \tag{3.20}$$

Now, since the tip of the vector $\vec{b}(t)$ is tracing a surface of a sphere of radius b centered around the center of mass, the arc that it traces at short time, $\Delta\vec{b}(t)$, can be considered as a vector in a tangential plane, so one can approximately write: $\theta^2 = \frac{1}{b^2}\left(\Delta b_x^2 + \Delta b_y^2\right) = \left(\int_0^t dt'\omega_x(t')\right)^2 + \left(\int_0^t dt'\omega_y(t')\right)^2$, where $\vec{\omega}(t) = \frac{1}{b}\frac{d\vec{b}(t)}{dt} = \frac{d\vec{\theta}}{dt}$ is the angular velocity of the hydrogen atom around the center of mass. Next, we us the identity

$$\begin{aligned}\left\langle\left(\int_0^t dt'\omega_x(t')\right)^2\right\rangle &= \left\langle\int_0^t dt'\int_0^t dt''\omega_x(t')\omega_x(t'')\right\rangle \\ &= 2\int_0^t (t-\tau)\left\langle\omega_x(0)\omega_x(\tau)\right\rangle d\tau. \end{aligned} \tag{3.21}$$

We finally arrive at a result [73],

$$\begin{aligned} C_1^s(t) &= \exp\left[-\int_0^t (t-\tau)\left\langle\omega_x(0)\omega_x(\tau)+\omega_y(0)\omega_y(\tau)\right\rangle d\tau\right] \\ &= \exp\left[-\frac{2}{3}\int_0^t (t-\tau)\left\langle\vec{\omega}(0)\cdot\vec{\omega}(\tau)\right\rangle d\tau\right]. \end{aligned} \tag{3.22}$$

Define the normalized angular velocity auto-correlation function as $\psi_R(t) = \left\langle\vec{\omega}(0)\cdot\vec{\omega}(t)\right\rangle / \left\langle\omega^2\right\rangle$, and its spectral density function as

$$Z_R(\omega) = \frac{1}{\pi}\int_{-\infty}^{\infty} e^{i\omega t}\psi_R(t)dt \tag{3.23}$$

which is normalized to 1 for ω from 0 to ∞. Therefore it is reasonable to make the approximation for the short-time part of the first order rotational correlation function as following:

$$C_1^s(t) = \exp\left[-\frac{4}{3}\left\langle\omega^2\right\rangle\int_0^\infty d\omega Z_R(\omega)\frac{1-\cos(\omega t)}{\omega^2}\right]. \tag{3.24}$$

We model the spectral density function by a simple gaussian-like function (see

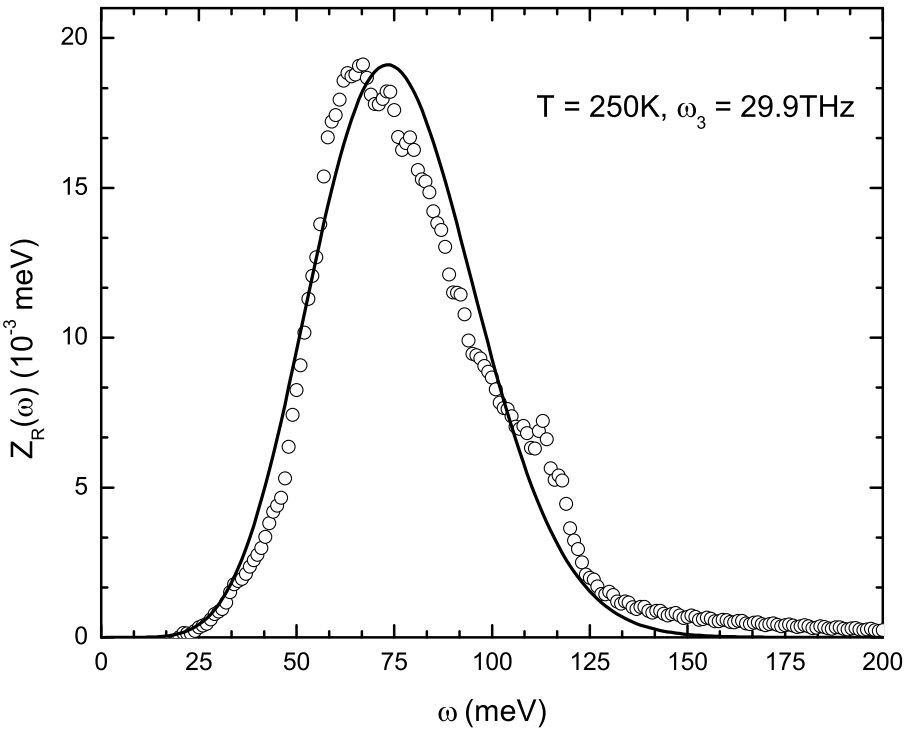

Figure 3-4: The spectral density function of the normalized angular velocity autocorrelation function $Z_R(\omega)$ at $T = 250$ K.

Fig. 3-4):

$$Z_R(\omega) = \frac{2\omega^6}{15\omega_3^6\sqrt{2\pi\omega_3^2}} \exp\left[-\frac{\omega^2}{2\omega_3^2}\right] \tag{3.25}$$

where $\sqrt{6}\omega_3$ denotes the peak position. The MD results show that this so-called hindered rotation peak, located approximated at 70 meV, is fairly independent of temperature. In Fig. 3-4, the open circles represent the results of the simulation and the solid line, the resulting fit by the model using Eq. 3.25. By applying Eq. 3.25 into Eq. 3.24, the short time approximation of the first order rotational correlation function can be written as:

$$\begin{aligned} C_1^s(t) &= \exp\left\{-\frac{2}{3}\langle\omega^2\rangle \int_0^\infty d\omega Z_R(\omega)\frac{1-\cos(\omega t)}{\omega^2}\right\} \\ &= \exp\left\{-\frac{4\langle\omega^2\rangle}{45\omega_3^2}\left[3\left(1-e^{\frac{-\omega_3^2t^2}{2}}\right) + 6\omega_3^2t^2e^{\frac{-\omega_3^2t^2}{2}} - \omega_3^4t^4e^{\frac{-\omega_3^2t^2}{2}}\right]\right\} \end{aligned} \tag{3.26}$$

This function describes the short-time behavior of the first order rotational correlation function. It starts from unity at $t = 0$, exhibits an oscillation at time 0.05 ps, and then decays to a flat plateau for times longer than 0.1 ps, determined by $\exp\{-4\langle\omega^2\rangle/15\omega_3^2\}$.

Analogous to the translational dynamics, the first order rotational correlation function can be separated in a short time harmonic libration in the cage and a long time relaxation of the cage. Therefore, the first order rotational correlation function can be written as the product of a short time libration and long time stretched exponential relaxation:

$$C_1(t) = C_1^s(t)\exp\left[-(t/\tau_R)^\beta\right] \tag{3.27}$$

where τ_R is the rotational relaxation time and β is the stretch exponent, same as in $F_T(Q,t)$ and the reason will be described later.

The whole picture resembles the relaxing cage model of the translational dynamics. At short time, the orientation of the central water molecule is fixed by the H-bonds with its neighbors. It performs nearly harmonic oscillations around the hydrogen bond

direction, described by $C_1^s(t)$. At longer times, the bonds break and the cage begins to relax, so that the water molecules can reorient themselves, losing memory of their initial orientation. Thus, the first order rotational correlation function eventually decays to zero by a stretched exponential relaxation.

We define a notation, $\mu(t) = \cos\theta(t)$. To calculate $C_2(t)$ and $C_3(t)$ from $C_1(t)$, we need a probability distribution function, $P(\mu, t)$, and we need to know its functional form. We shall guess the distribution function based on maximization of the informational entropy subjected to the condition that we know $C_1(t)$ [71]. This method is very effective at short times, corresponding to the harmonic libration. According to the scheme, the distribution function is given by

$$P(\mu, t) = e^{\alpha+\beta\mu}. \tag{3.28}$$

Because $\int d\Omega P(\mu, t) = 1$,

$$e^{\alpha} = \frac{1}{2\pi}\frac{\beta}{e^{\beta} - e^{-\beta}}, \tag{3.29}$$

$$C_1(t) = \int d\Omega e^{\alpha+\beta\mu}\mu = -[1/\beta(t)] + \coth\beta(t). \tag{3.30}$$

Then the higher order correlation functions can be determined from $C_1(t)$ using Eqs. 3.28, 3.29 and 3.30. The connection of $C_1(t)$ to the higher order rotational correlation functions is given in terms of $\beta(t)$. The results are:

$$C_2(t) = 1 - [3/\beta(t)]\, C_1(t), \tag{3.31}$$

$$C_3(t) = -\frac{5}{\beta(t)} + \left[1 + \frac{15}{\beta(t)}\right] C_1(t). \tag{3.32}$$

3.2.6 The validity of the theory of the rotational correlation functions

To explain the validity of the theory of the rotational correlation function, we focus on the validity of $C_1(t)$ as given by Eq. 3.24 and Eq. 3.27. Since the short-time behavior of the first-order rotational correlation function, $C_1^s(t)$, is essentially determined by the spectral density function of the normalized angular velocity autocorrelation function, $Z_R(\omega)$ [Eq. 3.24], we show in Fig. 3-4 the MD data of $Z_R(\omega)$ and its representation by the analytical function, $\left[2\omega^6/(15\omega_3^6\sqrt{2\pi\omega_3^2})\right]\exp\left[-\omega^2/(2\omega_3^2)\right]$. It is obvious that a broad band is peaked at ~ 65 meV for the MD data. In the gaussian representation by Eq. 3.25, the peak position is at $\sqrt{6}\omega_3$. We note that this analytical function is a fair representation of the spectral density function.

Next, we show that $Z_R(\omega)$ is part of the spectral density function of the hydrogen atom. Since we know that

$$\vec{v}_H(t) = \vec{v}_{CM}(t) + \vec{v}_R(t) \tag{3.33}$$

and

$$\vec{v}_R(t) = b\vec{\omega}(t), \tag{3.34}$$

we get the relation

$$\langle \vec{v}_H(0) \cdot \vec{v}_H(t) \rangle = \langle \vec{v}_{CM}(0) \cdot \vec{v}_{CM}(t) \rangle + b^2 \langle \vec{\omega}(0) \cdot \vec{\omega}(t) \rangle \tag{3.35}$$

in which we neglect the cross terms because they are very small compared with the others at short time. And since

$$Z_H(\omega) = \frac{1}{\pi}\int_{-\infty}^{\infty} e^{i\omega t}\frac{\langle \vec{v}_H(0) \cdot \vec{v}_H(t) \rangle}{\langle {v_H}^2 \rangle}dt, \tag{3.36}$$

$$Z_{CM}(\omega) = \frac{1}{\pi}\int_{-\infty}^{\infty} e^{i\omega t}\frac{\langle \vec{v}_{CM}(0) \cdot \vec{v}_{CM}(t) \rangle}{\langle {v_{CM}}^2 \rangle}dt \tag{3.37}$$

one can safely write

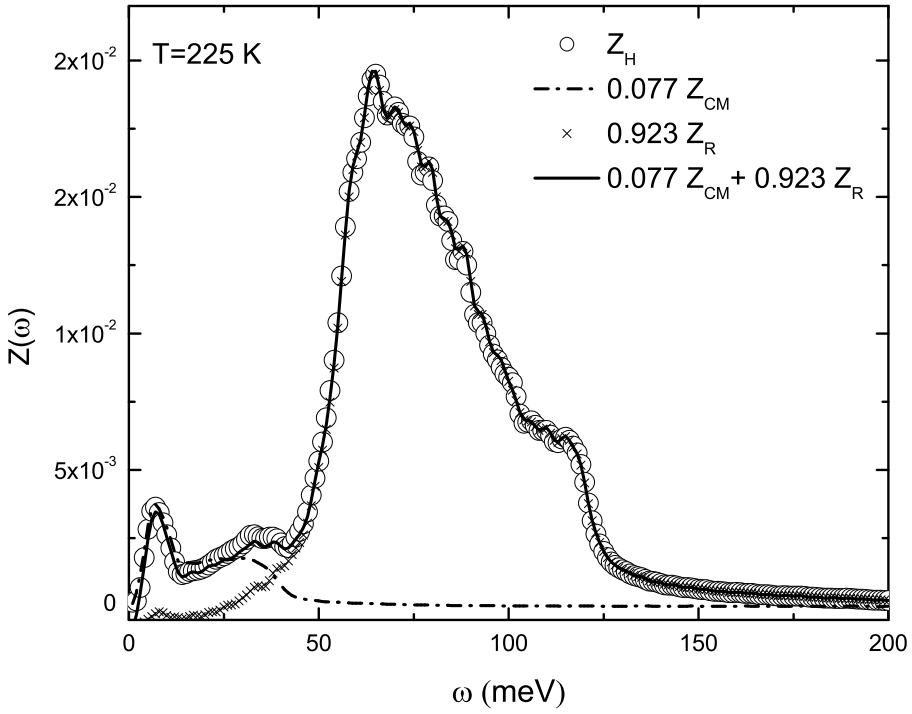

Figure 3-5: The spectral density function of the normalized velocity autocorrelation function of the hydrogen atoms $Z_H(\omega)$, and its decomposition into the weighted sum of $Z_R(\omega)$ and $Z_{CM}(\omega)$, where the latter quantity represents the spectral density function of the normalized center of mass velocity autocorrelation function.

$$Z_H(\omega) \simeq \alpha Z_{CM}(\omega) + \beta Z_R(\omega) \tag{3.38}$$

where

$$\alpha + \beta = 1.$$

In Fig. 3-5 we plot MD results for $Z_H(\omega)$ and its decomposition into sum of $Z_{CM}(\omega)$ and $Z_R(\omega)$ for $T = 225$ K. It is to be noted that the prominent peak at 65 meV, the so-called hindered rotation peak, hardly shifts as a function of temper-

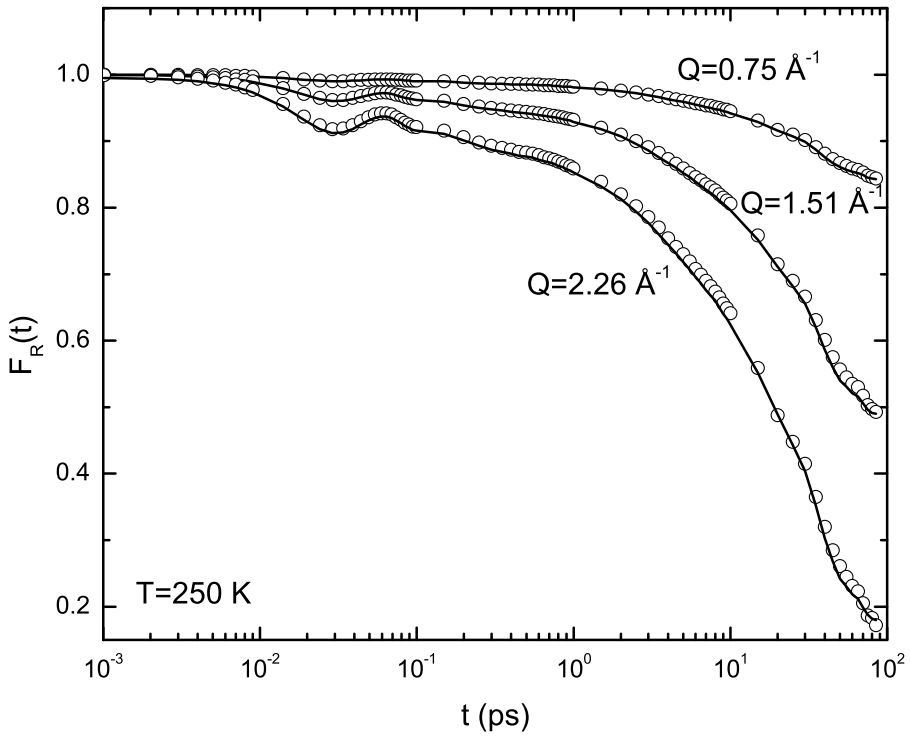

Figure 3-6: The rotational intermediate scattering function $F_R(Q,t)$ vs time at three Q values and at $T = 250$ K. From top to bottom, $Q = 7.54$ nm^{-1}, 15.1 nm^{-1}and 22.6 nm^{-1}.

ature. From the inspection of the figure, it is obvious that the two low frequency peaks of the hydrogen density of states are translational in character and the prominent high frequency peak belongs to rotations in character. In the literature, the latter peak is often called the hindered rotation peak, which is clearly associated with the oscillation of the hydrogen atom perpendicular to its hydrogen bond.

After applying the theory for $C_1^s(t)$ into $C_1(t)$ and derive $C_2(t)$ and $C_3(t)$ through $C_1(t)$, we are now ready to compute the rotational ISF using Sears expansion [Eq. 3.15]. Fig. 3-6 shows the rotational ISF calculated by MD at three Q values and their computation by Sears expansion using the MD generated $C_1(t)$, $C_2(t)$ and $C_3(t)$. The

open circles represent simulated $F_R(Q,t)$ at each Q value; the solid lines, the results computed by Sears expansion Eq. 3.15 up to fourth order term using simulated $C_1(t)$, $C_2(t)$ and $C_3(t)$. For all the three Q values, One sees good agreements between the two, indicating that up to $Q = 2.26$ Å^{-1}, our theoretical model for the rotational correlation functions are valid and the Sears expansion can be safely truncated at the fourth term.

3.2.7 The coupling of the translational and rotational dynamics

It has been clearly shown, using MD simulation, that translational and rotational dynamics are strongly coupled [22]. In fact, the long time behavior of the first, second, and third order rotational correlation functions, $C_1(t)$, $C_2(t)$, and $C_3(t)$, coincides with the long time behavior of the ISF of the center of mass at three specific Q values, Q_1^*, Q_2^*, and Q_3^*, independent of temperature [65, 74]. Even though the model uses the decoupling approximation, which neglects translational-rotational correlations, we impose the same stretch exponent, β, for both the translational ISF and the first order rotational correlation function. Therefore, at a specific Q^*, the long time decay of $F_T(Q^*,t)$ and $C_1(t)$ coincide: $\exp\left[-\left(t/\tau_T(Q^*)\right)^\beta\right] = \exp\left[-\left(t/\tau_R\right)^\beta\right]$, where Q^* is given by:

$$Q^* = \frac{1}{a}\left(\frac{\tau_0}{\tau_R}\right)^{1/\gamma} \tag{3.39}$$

Fig. 3-7 is the MD generated Q^*. It is between 1.0 and 1.2 at all temperatures, which could be seen as temperature-independent.

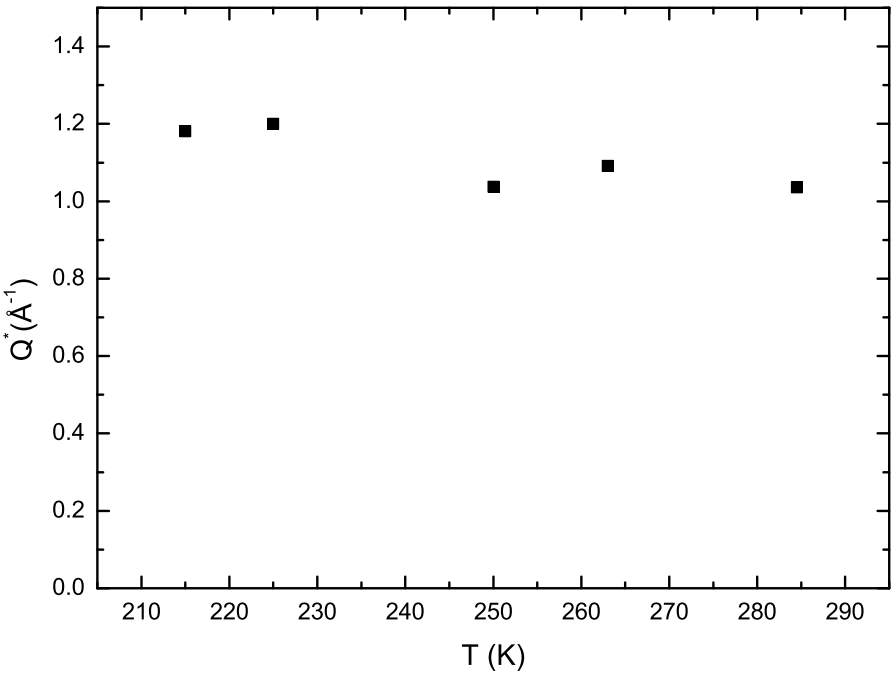

Figure 3-7: MD results for temperature dependence of the parameter Q^*.

3.3 Application of Two-Step Relaxation to Confined Water

It is likely that water confined in a capillary, only a few molecular diameters wide, has physical properties different from those of bulk water. In particular, its structure is significantly affected by the shell formation and the hydrogen bonding in the outer layer[2]. However, the main features of the RCM are the separation of the short-time and long-time dynamics and the generalization to a non-exponential behavior at long time, represented by the α-relaxation. The short-time dynamics is calculated according to the harmonic approximation, taking into account the experimentally observed three peak structure in the density of states of hydrogen atoms both in bulk water and in confined water in vycor glass [22, 26, 75]. The use of a stretched exponential relaxation function at long time accounts for the experimentally observed α-relaxation in supercooled bulk water and water in vycor glass [41]. In fact, MD simulation of water confined in 40 Å redius vycor pores clearly shows the existence of a two-step relaxation, namely a short time β-relaxation followed by a long time α-relaxation [26, 27]. Therefore, the main features of the RCM model should be applicable to water confined in nanoporous matrices as well as in bulk supercooled water.

Experimentally, we show in Fig. 3-8 a comparison of water confined in two systems. One is MCM-41-S-14 with 14 Å pore size, and the other one is a Vycor glass with 50 Å pore size, close to bulk water. The latter is taken by using Eq. 3.13 and Eq. 3.14 to fit the data in Ref. [29]. It is seen that the two sets of data agree with each other to within the experimental error. The only difference in the two cases is the limit to which water can be supercooled without freezing.

[2]The outer layer means the layer approximately 5 Å close to the surface.

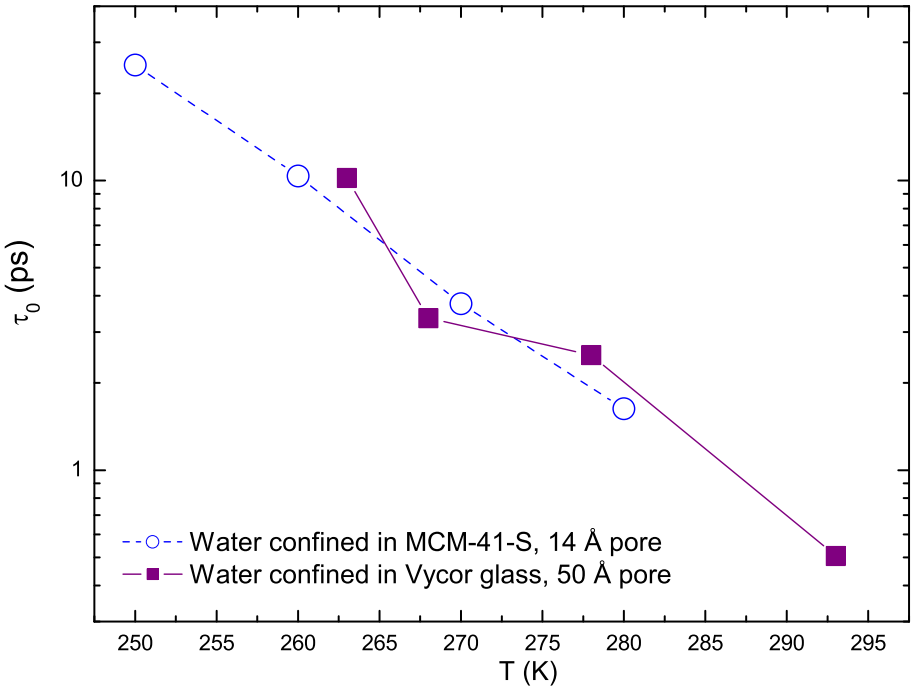

Figure 3-8: Comparison of the translational relaxation time parameter τ_0 for water confined in MCM-41-S-14 and water confined in Vycor glass with 50 Å pore size, which is closer to bulk water.

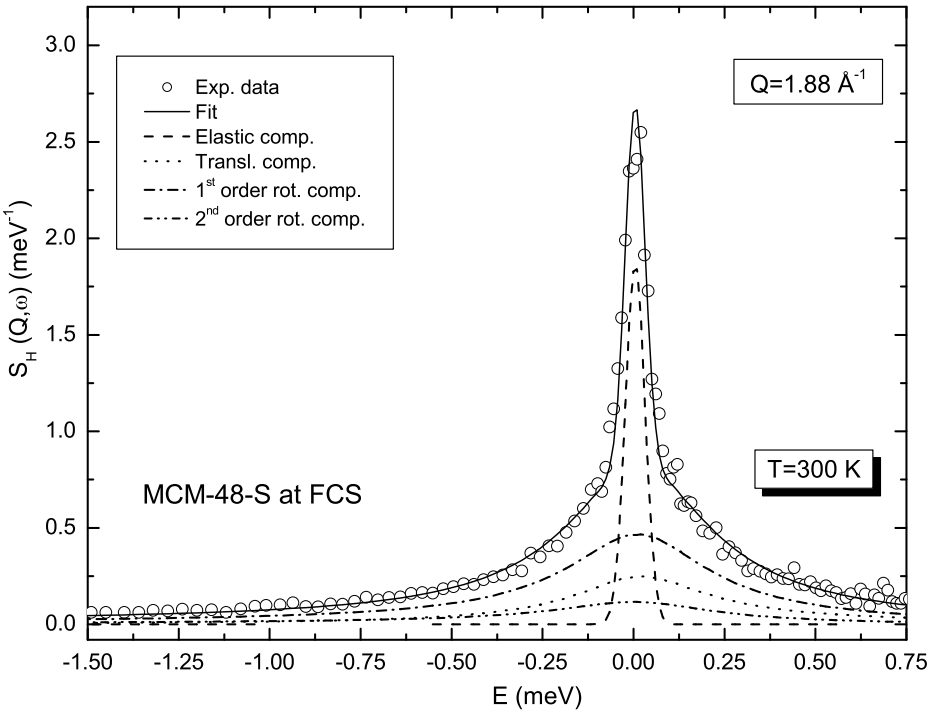

Figure 3-9: A typical QENS spectra from the MCM-48-S hydrated sample at $T = 300$ K, at $Q = 1.88$ Å^{-1}. Data were collected using FCS.

3.4 Data Analysis

Fig. 3-9 is an example of comparison of a recorded experimental spectrum with the fitted result using the RCM model. Error-bars are not shown for the sake of clarity of the figure; the scatter of the nearby data points furnishes an idea of the error. The lines show the different components of the data analysis: the continuous line represents the result of the fit; the dashed line is the elastic component; the dotted, dash-dot, and dash-dot-dot lines represent contributions to the scattering from the first three terms of the Sears expansion, respectively. The data, collected using FCS, refers to a sample of MCM-48-S-27 at $T = 300$ K, at $Q = 1.88$ Å^{-1}. It is seen that the agreement between the model and the experimental data is satisfactory throughout

the entire spectral range.

As shown in Fig. 3-9, a pronounced elastic component is superimposed on the quasielastic broadening. The presence of this quasielastic component is clearly detectable at most temperatures and Q, even with the broad resolution of FCS. The elastic contribution is mainly due to the scattering of hydrogen atoms in surface silanol (Si-O-H) groups [28]. The dangling O and H atoms of water molecules are connected to the surface Si atom to form a silanol group. In this silanol group, the H atom is not fixed, but is constrained to move in a circle in the surface to keep the O-H bond length and the Si-O-H angle constant. It is known that for the hydroxylated silica surface, surface solvent hydrogen bonding is stronger than interactions in the bulk solvent, with the nearest solvent layer interacting specifically with up to three surface hydroxyl groups. Therefore the strong interactions between water molecules and the silanol groups should be taken into account in our analysis as well.

As temperature decreases, the dynamics of water slows down markedly, and as a result, it is more difficult to resolve the quasielastic component even by the highest resolution QENS spectrometer. The bulk of the fluctuations are so slow that they could be seen as immobile by the QENS spectrometers and contributing to the elastic component. So that the elastic contribution increases as temperature decreases. It has been also found that the dynamics of water in nanoporous materials at supercooled temperature is better described by a distribution of relaxation times than a single average relaxation time.

Defining the magnitude of the wave vector transfer Q, corresponding to the scattering angle θ at the elastic channel as $Q_0 = [4\pi \sin(\theta/2)]/\lambda$, we can analyze the experimental data according to the following equation:

$$S(Q,\omega) = pR(Q_0,\omega) + (1-p)FT\{F_H(Q,t)R(Q_0,t)\} \tag{3.40}$$

where p is the area of the elastic component, $F_H(Q,t)$ is the ISF of hydrogen atoms, and $R(Q_0,t)$ is the Fourier transform of the experimental resolution function, $R(Q_0,\omega)$.

Taking the weight of the elastic component as a fitting parameter, we obtain the temperature dependent values for p. However, in this way we were trying to evaluate contributions from the hydrogen atoms of surface silanol groups, the water molecules interacting strongly with surface silanol groups and some of the very slow bulk water molecules. At temperature values lower than 270 K, the area of the elastic component seems to increase, whereas for $T \geq 270$ K a plateau is reached. The fast increase as lowering temperature is obviously connected to the slowing down of water dynamics. In the mean time, the plateau value is then the scattering due to the hydrogen atoms of surface silanol groups, without the contribution of bulk water and the water molecules interacting strongly with surface silanol groups. The surface silanol groups are so well organized and strong that they may be seen as temperature independent. We can find as well that even if FCS and DCS results agree very well, a sudden jump occurs when the data from HFBS are considered as well. This occurrence is due to the different resolution functions, more than one order of magnitude sharper than for DCS. In the ideal case, the area of the elastic component would be resolution independent, if two clearly separated relaxation times can be identified with one inside the experimental time window and the other corresponding to virtually immobile particles. However, experimentally, we expect a continuous distribution of relaxation times in supercooled water, encompassing the dynamics of water in the inner part and on the surface of the pores. Therefore, the value of p is strongly dependent on the time-window cut-off. For this reason, to obtain consistent results, we have fixed p to its plateau value: $p = 0.12$ and 0.08 in the case of MCM-48-S and MCM-41-S, respectively, when analyzing the data from different spectrometers. We argue that, without introducing an arbitrary cut-off, it is impossible to identify a population of molecules whose dynamics is much slower than the resolution of the instrument. More consistent results from different instruments can then be obtained by assuming a single distribution of relaxation times for the whole water population. It would be expected that p of MCM-48-S should be smaller than of MCM-41-S since the water content in the MCM-48-S sample is slightly higher than in the MCM-41-S case. However, the fixed plateau value for MCM-48-S is slightly higher than MCM-41-S, because the amount of silanol groups

is larger in the sample with larger surface area (MCM-48-S).

The quasielastic broadening has been analyzed according to the RCM as described in the previous section. $F_H(Q,t)$ is described in terms of ten parameters (from Eq. 3.4, 3.5, 3.11, 3.13, 3.15, 3.26, 3.27, 3.31, 3.32 and 3.40): C, ω_1, ω_2, τ_0, γ, β, ω_3, τ_R, $\langle\omega^2\rangle$ and p. Five of them are related to the short-time dynamics, namely C, ω_1, ω_2, ω_3, and $\langle\omega^2\rangle$. The short-time dynamics is not strongly temperature dependent, according to MD simulation results. On the other hand, the quasielastic broadening is mostly determined by the long-time dynamics. For this reason, we have fixed the values of C, ω_1, ω_2, and ω_3 according to the results of our MD simulations. This procedure is reliable. In fact, MD simulation results on the short-time dynamics can be compared with the experimental results from inelastic neutron scattering, and the agreement is very satisfactory [21, 22]. $\langle\omega^2\rangle$ has been fixed according to the equation $\langle\omega^2\rangle = k_BT/I$, through an estimation of the momentum of inertia of the water molecules. This value is in agreement with the results of MD simulations [22] and of the combined analysis of QENS and Inelastic Neutron Scattering (INS) spectra [66].

The remaining parameters, namely p, τ_0, γ, τ_R, and β, can be determined from the analysis of the QENS spectra. However, in this and following chapters, we report the results of our analysis with the value of p fixed to its plateau value. Therefore, since the fitting parameters are Q independent, we fit the experimental $S(Q,\omega)$ surface (both ω- and Q-dependence) using just four fitting parameters. We took into account the first three terms of the Sears expansion. We actually fitted constant angle spectra, taking into account the dependence of Q on the energy transfer, E:

$$Q = \sqrt{2m_n \left[2E_i - E - 2\cos\theta\sqrt{E_i\left(E_i - E\right)}\right]} \tag{3.41}$$

where m_n is the mass of the neutron and E_i is the energy of the incident neutrons.

In Fig. 3-10, we show as an example three spectra collected using FCS, DCS, and HFBS. The continuous, dash, dot, dash-dot and dash-dot-dot lines represent the total fit, the elastic component and the contributions from the first three terms of the Sears

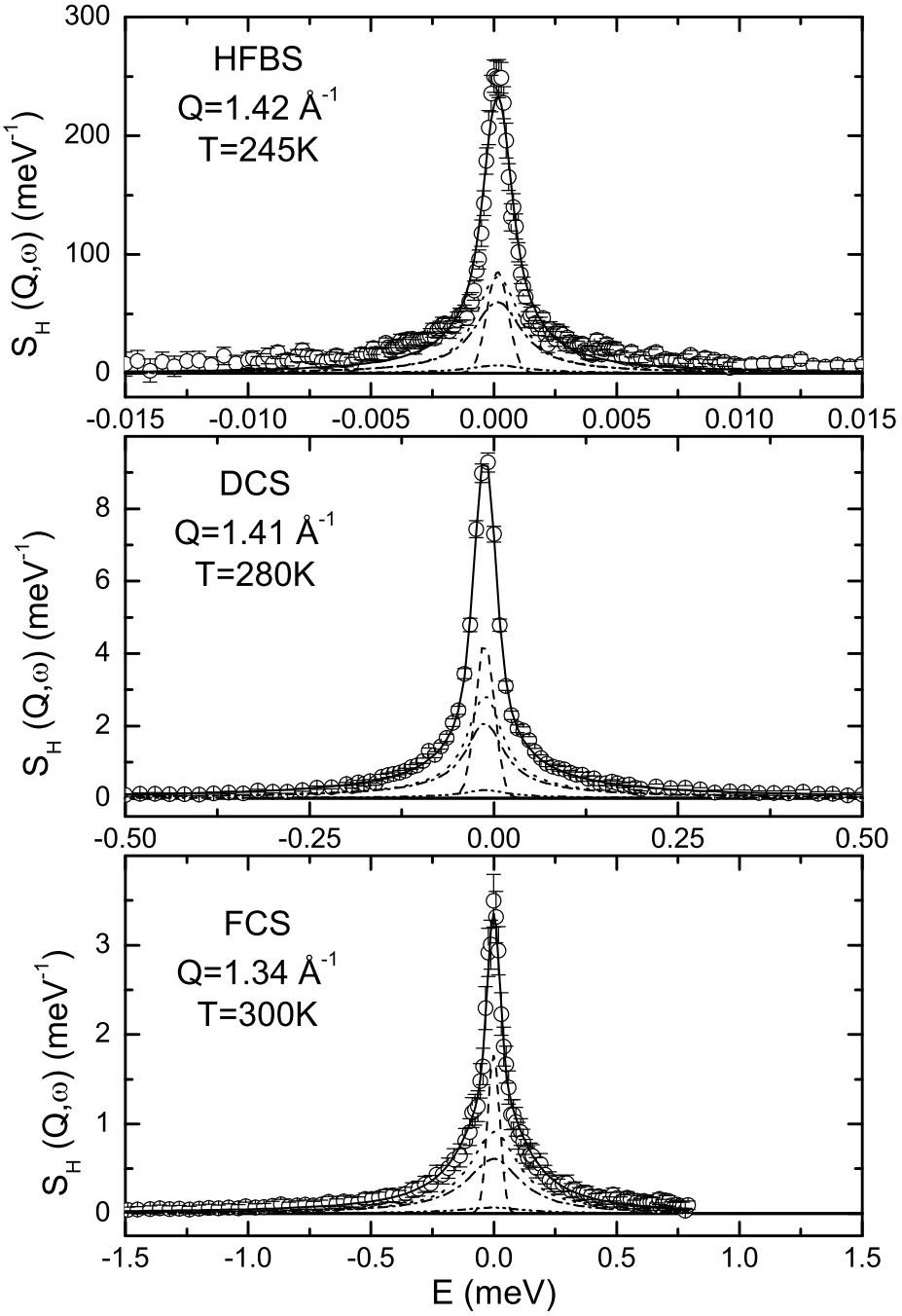

Figure 3-10: Comparison of the typical QENS spectra of the MCM-48-S sample from the three different spectrometers, at three different temperatures.

expansion, respectively. From the figure, the progressive sharpening of the quasielastic broadening as temperature is lowered can be noticed. The 1 μeV resolution of HFBS is necessary to obtain useful data at $T \leq 250$ K, even if the resulting energy window is quite small. As the broadening is strongly temperature dependent, the data have been fitted in different energy windows for the three spectrometers. FCS and DCS data have been analyzed in the ranges -5 meV $\leq E \leq$ 0.8 meV and -2 meV $\leq E \leq$ 0.9 meV, respectively. Such big ranges are necessary to the analysis of the rotational components, whose wings are very large at the high Q values. In any spectra, no appreciable background has been noticed. HFBS energy window is from -30 μeV to 30 μeV. In this small interval, the Q value can be considered equal to the zero energy transfer value, Q_0, in the whole range.

As can be seen, the fit of RCM to the experimental spectra is very good in all investigated cases. It is remarkable that using four parameters we were able to reproduce the data from 11 (FCS), 9 (DCS), and 7 (HFBS) constant angle spectra.

3.5 Low Q Approximation

From our early analysis, we find out that the rotational dynamics is much slower than the translational dynamics of supercooled water. Thus it is hard, for the experimental tools provided nowadays, to detect the rotational dynamics and extract useful information. For this reason, when we continue our exploration on slow dynamics of supercooled water, especially under high pressure conditions, we focus on our data analysis at low Q part.

By considering only the spectra with wave vector transfer $Q < 1.1$ Å^{-1}, we can safely neglect the contribution from the rotational motion of water molecule in ISF [21].

The RCM described ISF of hydrogen atoms is then written as:

$$F_H(Q,t) \approx F_T(Q,t)$$

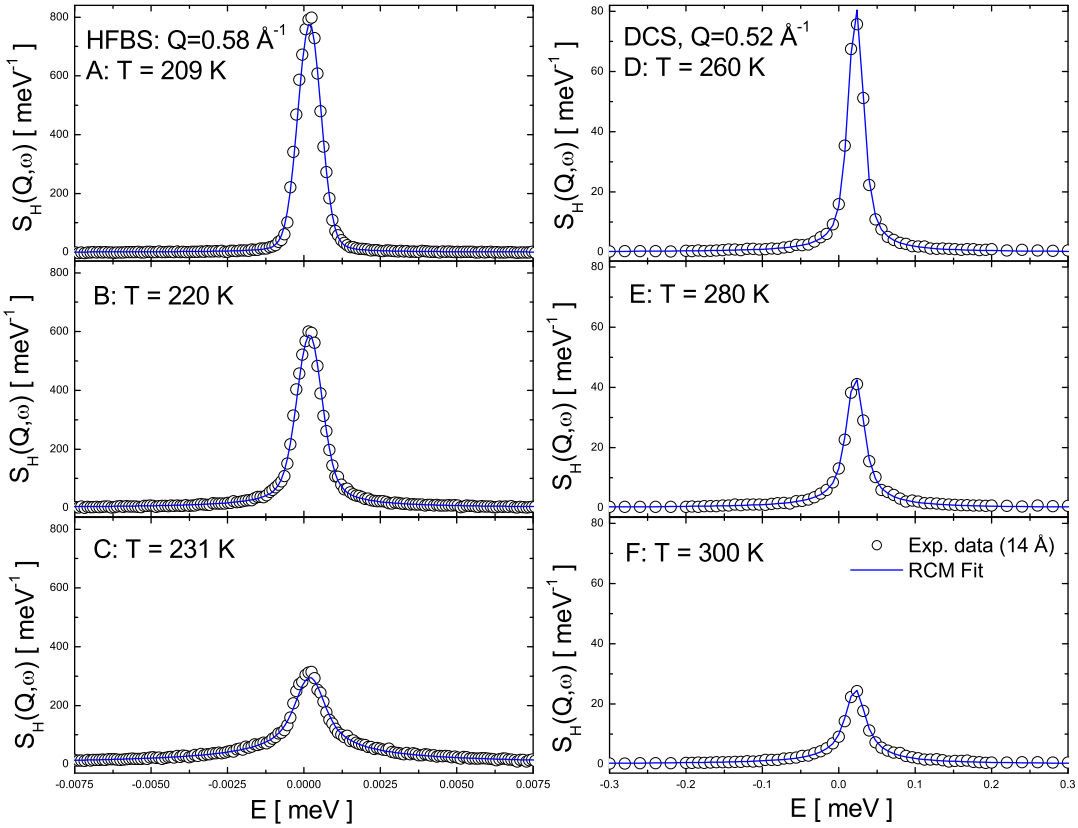

Figure 3-11: QENS spectra measured at $Q = 0.58$ Å^{-1} for HFBS and $Q = 0.582$ Å^{-1} for DCS , at a series of temperatures.

$$= \quad F^S(Q,t)\, exp\left[-\left(t/\tau_T(Q)\right)^{\beta}\right], \tag{3.42}$$

and

$$\tau_T(Q) = \tau_0 \left(0.5Q\right)^{-\gamma}. \tag{3.43}$$

We show in Fig. 3-11, as an example, two complete sets (temperature series) of QENS area-normalized spectra taken at HFBS and DCS spectrometers. It is obvious, from the spectra, that for the low Q data, taking into account only the translational dynamics of supercooled water is an appropriate approximation for the study of the

broadening of the quasi-elastic peaks. More spectra illustrating the method of data analysis will be shown later.

Chapter 4

Average Translational and Rotational Relaxation Times of Supercooled Water at Ambient Pressure

4.1 Definition of Fragility and Different Laws for Relaxation Times

Glass is an amorphous solid resulted from supercooling or compressing a fluid in such as way that it bypasses crystallization. Many types of materials are capable of glass formation, including molecular liquids, polymers, metal alloys and molten salts. Given such diversity of materials, a general scheme by which different glass-forming materials can be systematically classified is useful. One such scheme is the classification of glass-formers according to their "fragility". Fragility measures the rate with which transport properties of a liquid, such as structural relaxation time, viscosity or the inverse self-diffusion constant, change as the glassy state is approached from the liquid side by lowering the temperature.

By convention, the glass transition temperature T_g is where the viscosity η reaches

a value of 10^{12} Pa $\cdot$ s or the structural relaxation time τ reaches 100 second. The approach to this large η or τ, however, differs from one liquid to another. When displayed in an Arrhenius plot of log η (or log τ) versus inverse temperature $1/T$, some liquids (such as silica) show a uniform, linear increase, while others display a much steeper dependence on $1/T$ (such as *o*-Terphenyl). The former are called 'strong' liquids, and the latter, 'fragile' liquids. Thus, the glassy liquid is called 'fragile' when its viscosity or relaxation time varies according to the so-called Vogel-Fulcher-Tammann (VFT) law: $\tau = \tau_1 \exp[DT_0/(T - T_0)]$, where T_0 is the temperature of apparent divergence of the relaxation time; and the magnitude of D gives the degree of fragility. The liquid is called 'strong' when the viscosity or relaxation time obeys Arrhenius law: $\tau = \tau_1 \exp[E_A/RT]$, where E_A is the energy barrier for the relaxation process, and R, the gas constant [76].

It is well known that water above 235 K is one of the most fragile liquids that have ever been studied [77]. Angell and coworkers [77] proposed that a 'fragile-to-strong' transition would occur at around 228 K at ambient pressure, based on a thermodynamic argument. But the bulk water nucleates into hexagonal ice at and below $T_H = 235$ K, so this transition falls in an inaccessible region of temperatures and it has not been observed directly so far [15]. By containing water in small cylindrical pores (pore size ≤ 18 Å) of MCM-41-S, we were able to circumvent the homogenous nucleation process and supercool water down to 160 K.

4.2 MD Simulated Average Translational Relaxation Times

In Fig. 4-1 we show the temperature dependence of the average translational relaxation time, $\langle \tau_T \rangle = (\tau_0/\beta)\,\Gamma\,(1/\beta)$, obtained from MD simulations of SPC/E water. The ISFs of C. M. at different temperatures, calculated from the MD trajectories, have been fitted according to the RCM, using Eqs. 3.11 and 3.13. We fit these results

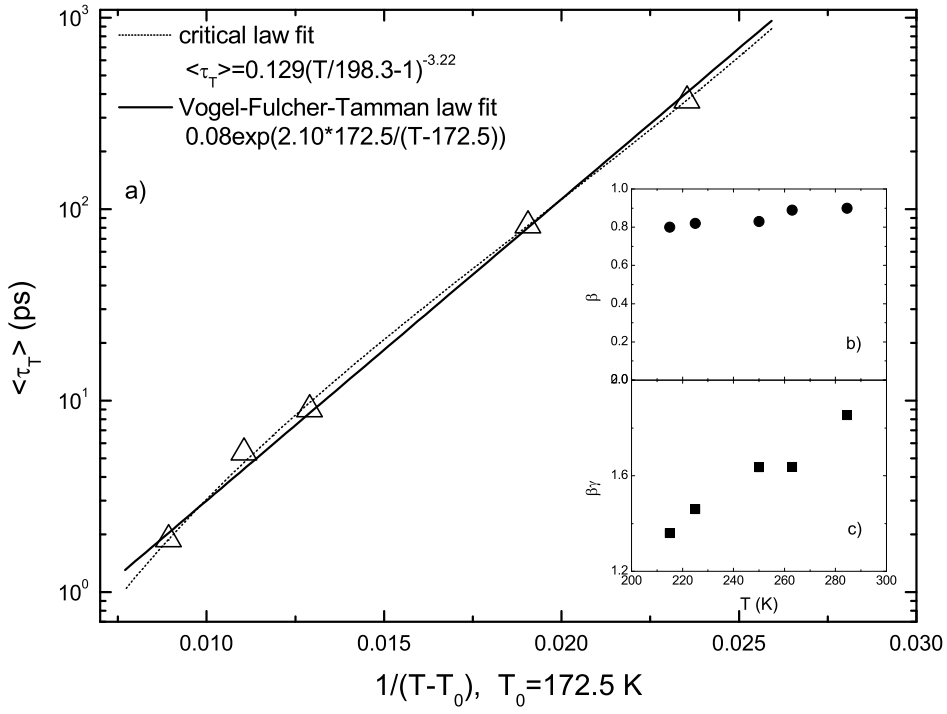

Figure 4-1: Temperature dependence of the average translational relaxation times as extracted from SPC/E water MD data. The inset shows the behavior of the stretch exponent β and of $\beta\gamma$.

with both critical law and the Vogel-Fulcher-Tamman law. It is well known that the diffusion coefficient of bulk water follows a critical behavior [7]. In our case, at low temperature, we cannot extract the diffusion coefficient from the average translational relaxation time, $\langle \tau_T \rangle = (\tau_0/\beta)\,\Gamma\,(1/\beta)$, because it is not Q^2-dependent. The obtained data follow the critical law: $\langle \tau_T \rangle \sim (T/198.3 - 1)^{-3.22}$. This result is in accordance with the reported temperature dependence of the self-diffusion coefficient for SPC/E water [24]: $D \sim (T/198.7 - 1)^{2.73}$. Both D and $\langle \tau_T \rangle$ follow a critical law in temperature, with similar T_c. Since SPC/E water temperature of maximum density is $T = 250$ K, there is a 27 K offset between the real and computer temperature. Therefore, the critical temperature obtained by MD simulations in this case correspond to $T \approx 225$ K in real water. In the mean time, the Vogel-Fulcher-Tamman (VFT) law shows a good fit to MD generated $\langle \tau_T \rangle$ as well. VFT law is a way to fit relaxation times close to the glass transition point. According to the VFT law:

$$\tau = \tau_1 e^{DT_0/(T-T_0)} \tag{4.1}$$

where τ_1, D and T_0 are constants. And τ_1 is a vibration time. T_0 is an ideal glass transition temperature. It is shown in Fig. 4-1 that $T_0 = 172.5$ K, corresponding to 200 K in bulk water. It is seen in the inset that β has slightly temperature dependence starting from 0.9 at 284.5 K down to 0.8 at 215 K. $\beta\gamma$ is the exponent determining the Q dependence of the relaxation time, τ_T. It is seen that at high temperature, the exponent starts from 2, signifying a free diffusion, and decreases linearly to value below 2, signifying a restricted diffusion.

4.3 MD Simulated Average Rotational Relaxation Times

To see the critical behavior of rotational dynamics, we have analyzed SPC/E water MD simulation trajectories to obtain $C_1(t)$ and $C_2(t)$. Their long time relaxation

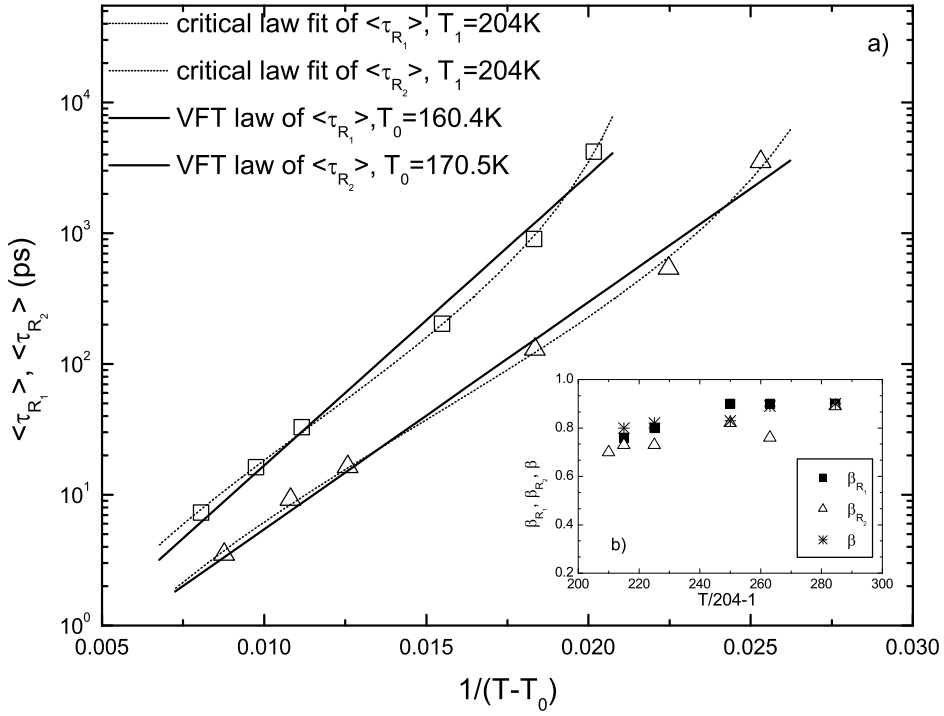

Figure 4-2: Temperature dependence of the average relaxation times for the first and second order rotational correlation functions as extracted from SPC/E water MD data. The inset shows the stretch exponents.

has been fitted to a stretched exponential function. Fig. 4-2 shows the obtained results. The data obey a critical law with $T_c^{MD} = 204$ K, which is close to the critical temperature found for the translational dynamics of SPC/E water. The data obey VFT law as well with $T_0(\langle\tau_{R_1}\rangle) = 160.4$ K and $T_0(\langle\tau_{R_2}\rangle) = 170.5$ K, which is near the value got from the average translational relaxation times, $T_0 = 172.5$ K, signaling an ideal glass transition at about 200 K (real temperature).

We show the β values for the fitting of $C_1(t)$ and $C_2(t)$, in Fig. 4-2 inset b). At the same time, the β values for the translational dynamics are shown as denoted β. Within the error limit, they can be considered coincident, which confirms the validity of the assumption, in the fitting algorithm, that $\beta_R = \beta$. Also we should note that the stretch exponents, β_{R_1} and β_{R_2}, are slightly Q dependent, approaching 1 in the limit $Q \to 0$. In QENS experiments, where this low-Q limit is not easy to be reached, β can be considered Q-independent.

4.4 Experimental Results of Supercooled Water confined in MCM-41-S at Ambient Pressure

In Fig. 4-3 we report, as an example, the spectra collected in the region of the fragile-to-strong (F-S) transition. The sharpening of the peak from the $T = 230$ to 225 K, being more noticeable than the one from 220 to 210 K, already suggests the existence of a transition. The normalized data were analyzed using Eq. 3.40. $F_H(Q,t)$ is calculated according to the equations of RCM. Both F_T^s and C_1^s were calculated using the parameters obtained from MD simulations, which are in agreement with experimental results [41]. Each series of constant angle spectra recorded at any investigated temperature (9 and 7 spectra in the case of DCS and HFBS, respectively) have been fitted altogether, using four (Q and ω independent) parameters, namely τ_T, τ_R , γ, and β, with satisfactory results. In the case of DCS the dependence of Q on ω has been taken into account. The parameter p represents the area of the elastic contribution arising from the glass matrix, determined from the high temperature spectra,

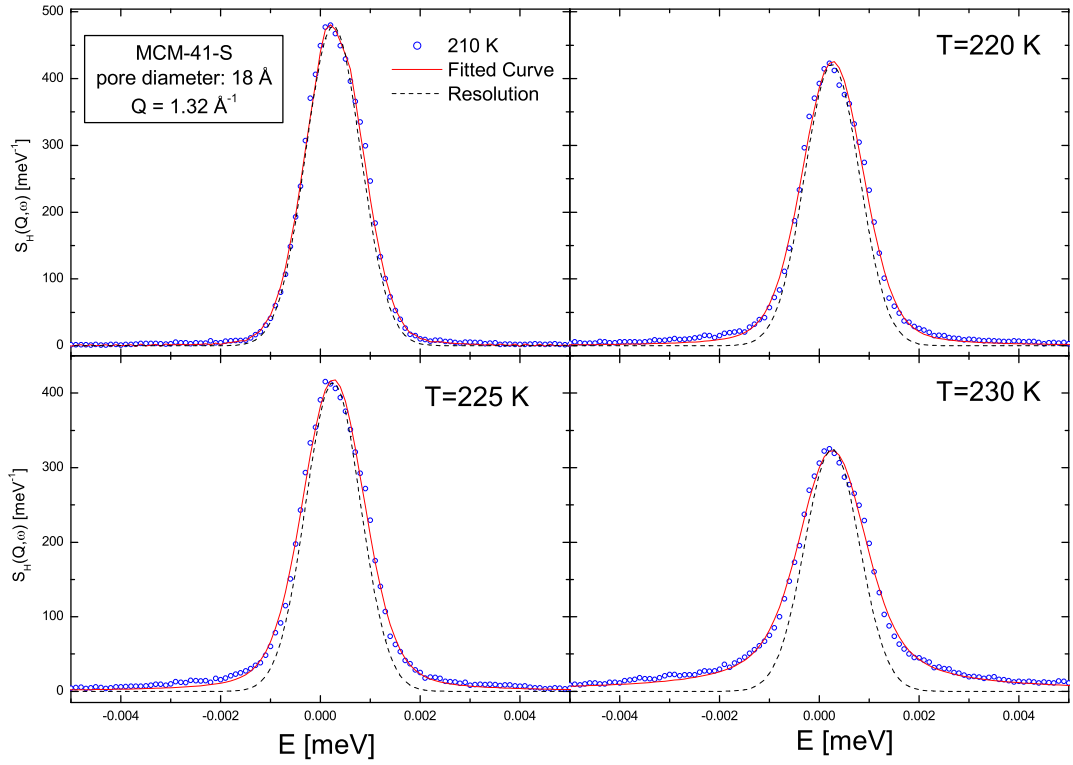

Figure 4-3: QENS spectra taken from HFBS at four temperatures, 230, 225, 220, and 210 K. The squares represent the real data taken from experiments; the solid lines represent the result of the fit; and the dash lines represent the Gaussian resolution function.

where it clearly superimpose on the quasielastic broadening. Also to be noted that the broadening of the experimental data over the resolution function, shown in all four panels of Fig.4-3, leaves enough dynamic information to be extracted by RCM.

The fitting of the data allowed us to extract the parameters describing the translational and rotational dynamics of water. Thus, we have been able to study the effects of confinement and temperature on hydration water in MCM nanoporous sieves.

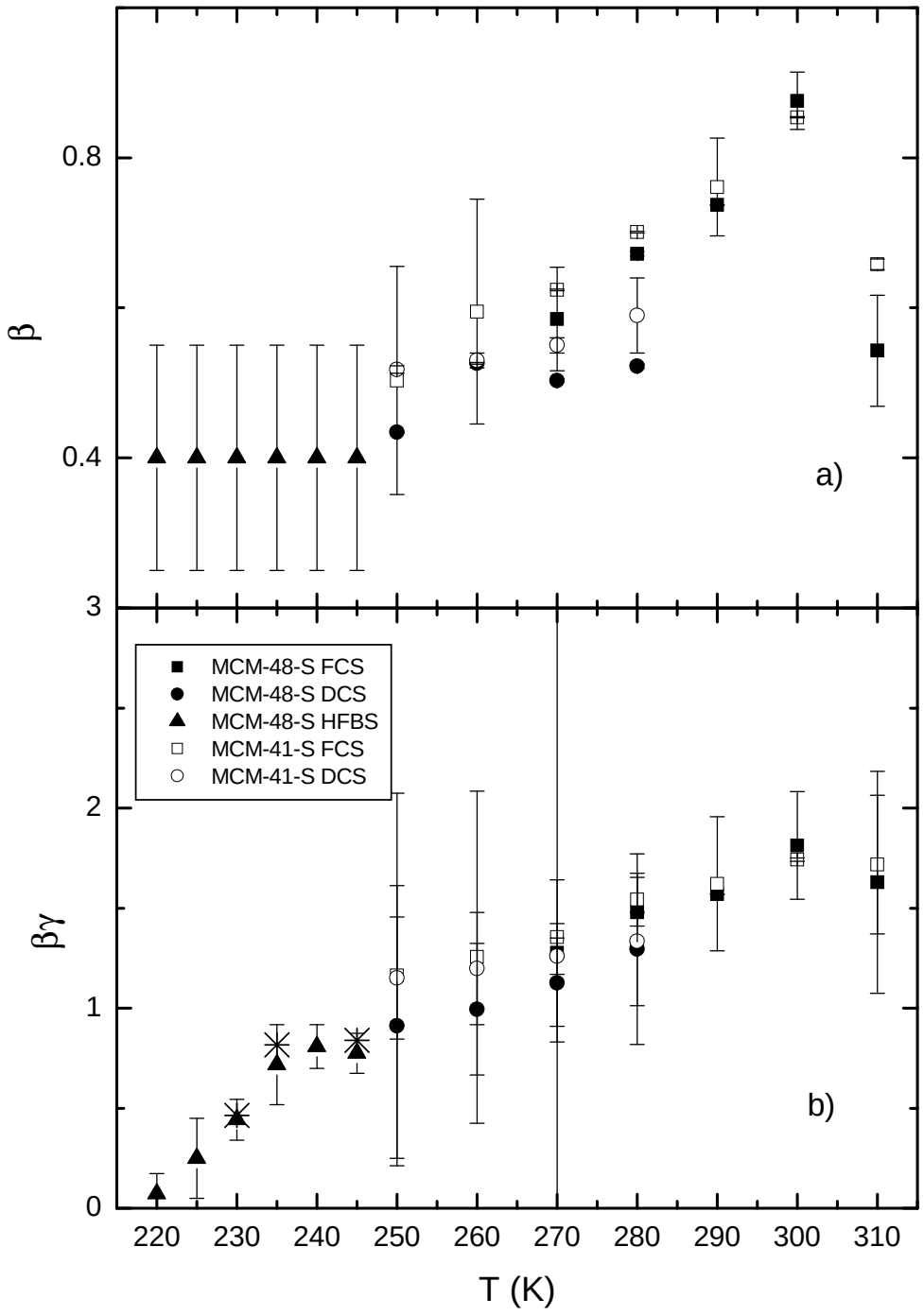

Figure 4-4: Temperature dependence of stretch exponent, β, and of the translational relaxation time Q-dependence power law exponent, γ. In panel b) the product $\beta\gamma$ is reported. In panel b) the asterisks are the results when beta is fixed to the value 0.4 in the analysis of HFBS results.

Fig. 4-4 reports the temperature dependence of the parameters β and $\beta\gamma$ obtained from the fitting procedure. In the measured temperature range, both DCS and HFBS spectra give $\beta \approx 0.5$, roughly constant in T. The product $\beta\gamma$ is the actual exponent of the Q-dependence of the ISF. In the previous analysis without fixing the values of p, we obtained values of β increasing with decreasing temperature. We had suggested that this occurrence was most probably due to a finite resolution effect. In fact, fixing p to the value corresponding to the scattering of the silica matrix, β decreases with the lowering of temperature. This behavior is in agreement with the results obtained by MD simulations and is more sound with the idea that upon supercooling the diffusive dynamics of a water molecule involves the cooperative rearrangement of the surrounding particles. This occurrence causes the non-exponentiality of the decaying function. As a matter of fact, when water is confined in nanoporous materials the translational long-time relaxation is a stretched exponential already at room temperature. HFBS data, in the temperature range 245 K to 220 K, are consistent with a low value (0.4) of β.

It is well known that a Fickian diffusive process has a Q^2 dependence. In hydration and supercooled water, since the diffusive process is somewhat obstructed, the average translational relaxation time follows a power law in Q, with a power exponent ≤ 2. In our previous analysis we actually found that at room temperature γ is ≈ 2, indicating a normal diffusive behavior, and that it progressively decreases with the lowering of temperature. This behavior was attributed to a reduced dimensionality of the diffusive process.

Recently, a series of papers have investigated in details the Gaussianity of the relaxation dynamics in polymers [78, 79, 80]. Very interesting results have been reported. In particular, many similarities between the behavior of polymers and of supercooled liquids, water in particular, have been found. It has been reported that the product $\beta\gamma$ is 2 at high Q and decreases above a critical Q value, Q_c. This indicates the transition from a gaussian to a non-gaussian behavior. In fact, $\beta\gamma$ is the power dependence of Q in the ISF of C. M.. If $\beta\gamma = 2$, the van Hove self-correlation function of C. M., $G_s^{CM}(r,t)$, which is the Fourier transform of $F_T(Q,t)$,

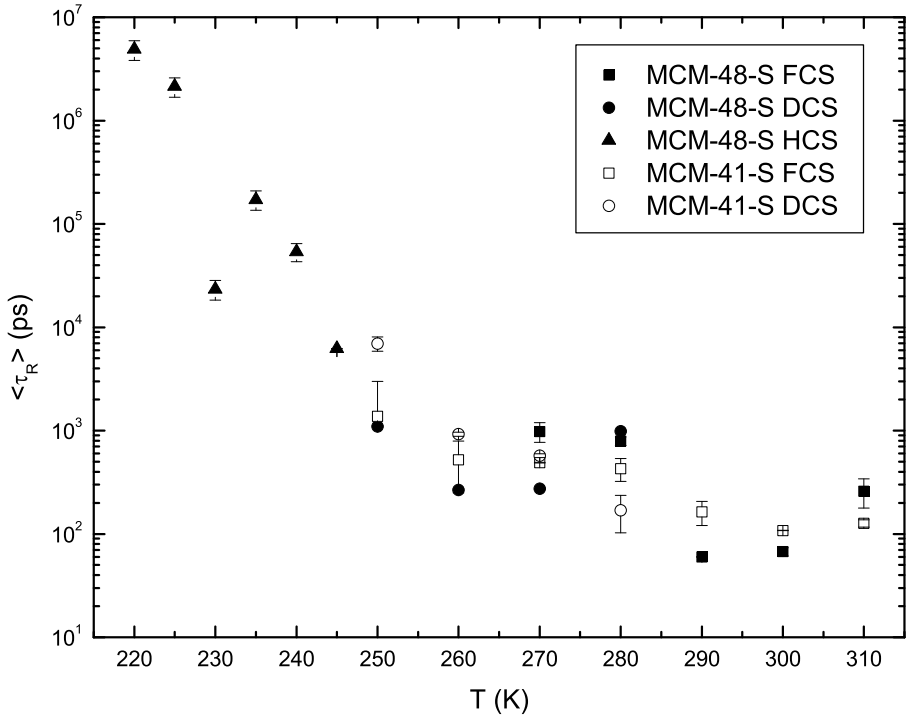

Figure 4-5: Temperature dependence of $\langle \tau_R \rangle$ as extracted from the analysis of the data taken using the three QENS spectrometers: FCS, DCS, and HFBS. Solid and open scatter show the results for the MCM-48-S (22 Å pore size) and MCM-41-S (25 Å pore size) matrix respectively.

is a Gaussian function. In water, the van Hove self-correlation function of C. M. has been investigated by MD simulations [24, 81]. Through the investigation of the non-gaussian parameter, α_2, it has been shown that $G_s^{CM}(r,t)$ is not-Gaussian at long times at supercooled temperatures.

Fig. 4-5 shows the average rotational relaxation time, $\langle \tau_R \rangle = (\tau_R/\beta)\,\Gamma\,(1/\beta)$, as obtained from the experimental results. In the temperature range $220\ \mathrm{K} < T < 310\ \mathrm{K}$, the average rotational relaxation time increases five orders of magnitude, showing a dramatic slowing down of the rotational dynamics. However, we could not succeed in fitting the data to a critical law or VFT law. These results are strongly affected

Table 4.1: Fitting parameters of experiments taken at ambient pressure.

Samples	T_0 (K)	D	τ_1 (ps)	E_A $(Kcal/mol)$	T_L (K)
Mac-41-S-10	190	1.58	0.0045	3.91	224
Mac-41-S-12	190	1.51	0.0086	3.51	227
Mac-41-S-14	170	4.62	0.0025	6.72	224
Mac-41-S-18	200	1.47	0.079	5.28	225

with finite resolution effects.

Fig. 4-5 compare the average rotational relaxation times for the two matrices. The size and morphology of the pores do not seem to affect the rotational dynamics, as the obtained data can hardly be considered different for the two samples. In fact, the rotation process of a water molecule takes place within a sphere of radius b from C. M., and is not directly affected by confinement within pores larger than 20 Å. However, it is reasonable to presume that confinement affects the rotational dynamics through translational-rotational coupling. In this case the pore dimensions are quite similar and $\langle\tau_R\rangle$ values in the two matrices tend to coincide.

Fig. 4-6 shows the temperature dependence of the average translational relaxation times, $\langle\tau_T\rangle = \frac{\tau_0}{\beta}\Gamma(1/\beta)$, where Γ is the gamma function, τ_T and β are the characteristic relaxation time and the stretch exponent of the translational dynamics, respectively (defined in Chapter 3). $\langle\tau_T\rangle$ has been fitted to a VFT law, $\langle\tau_T\rangle = \tau_1 \exp\left[DT_0/(T-T_0)\right]$, for $T \geq 230$ K, obtaining parameters for different pore sizes listed in Table 4.1. A critical law, which is usually used for bulk supercooled water, would fit the data above 240 K, but deviates from the data below 240 K [83]. At $T \leq 225$ K, there is a sudden change in the slope of the $1/T$ dependence of $log(\langle\tau_T\rangle)$, which can be fitted with an Arrhenius law, with activation energies E_A reported in Table 4.1. Note that this transition happens in the same temperature range where the drop in $\beta\gamma$ occurs. Our best fit gives us T_0 values higher than the normal glass transition temperature of water $T_g = 165$ K, as recently proposed [82], and D values

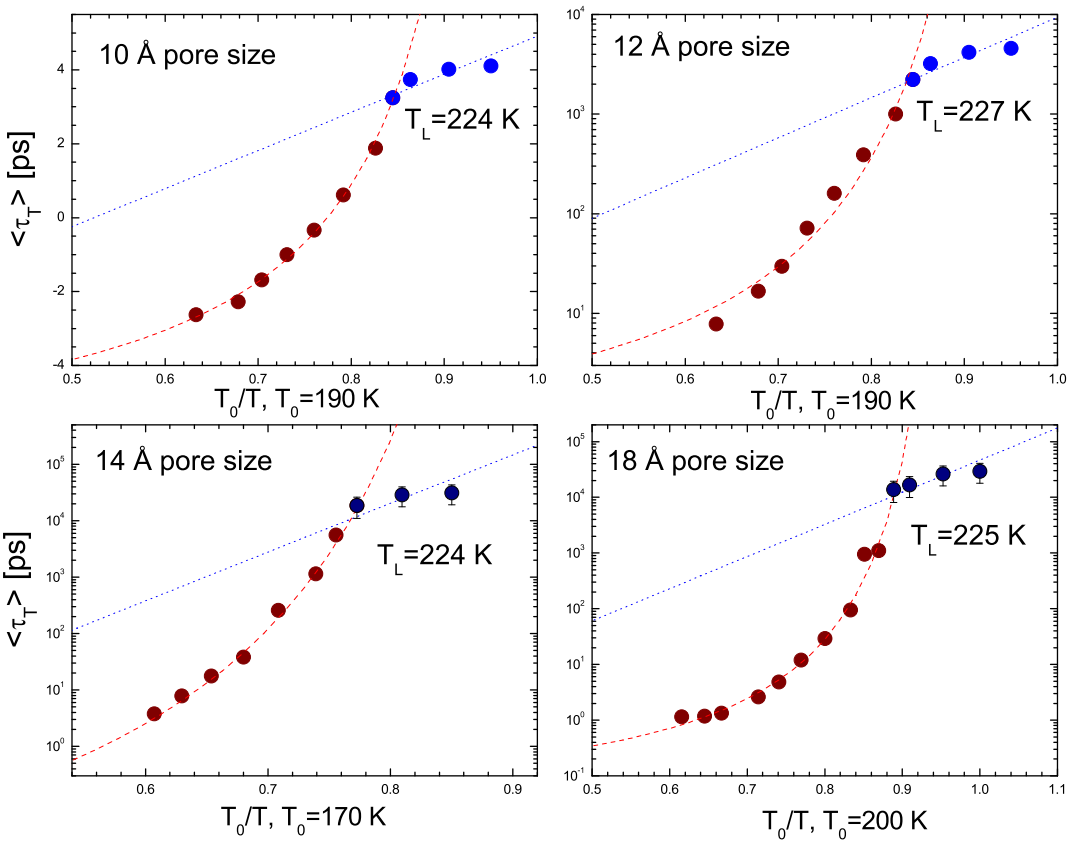

Figure 4-6: Temperature dependence of $\langle \tau_T \rangle$ plotted in $log(\langle \tau_T \rangle)$ vs T_0/T scale. Data at ambient pressure from H_2O hydrated in MCM-41-S with different pore sizes are shown in different panels. Solid circles are the experimental data; the dash lines are the VFT law fit of the experimental data; and the dot lines are the Arrhenius law fit of the experimental data.

indicating a very fragile liquid. Our finding is in agreement with the known properties of water in the melting and supercooled region. In fact, a fragile-to-strong (F-S) liquid transition in water was proposed [77] on the basis of the determination of the fragility of water near the melting and glass transition temperatures: near T_g water is a very strong liquid, whereas in the supercooled region it is the most fragile one. A strong experimental support to this hypothesis was already given by a dielectric relaxation investigation of water confined in vermiculite clay [15], although the actual transition was not observed. The F-S transition will be discussed in more details in Chapter 5. It is to be noted that the transition temperature T_L for different pore size samples, reported in Fig. 4-6 and Table 4.1, does not change within error bars. Thus we propose that when pore size of confinement is sufficiently small, ≤ 18 Å, the F-S transition is size-independent, which means that F-S transition is a widely existed property of supercooled water in small confinement. We will discuss more about this topic in Chapter 5.

Chapter 5

Pressure Dependence of the Average Translational Relaxation Time

As explained in Chapter 2, we performed QENS experiments on both HFBS and DCS instruments at NIST NCNR, using the same high pressure system. We collected spectra for fully hydrated MCM-41-S-14, with 14 Å pore size, spanning 10 pressures: ambient, 100, 200, 400, 800, 1200, 1400, 1600, 2000, and 2400 bars.

In addition to QENS experiments taken at NIST NCNR, an Inelastic Neutron Scattering (INS) measurement of the librational band of water was carried out at High-Resolution Medium-Energy Chopper Spectrometer (HRMECS) at the Intense Pulsed Neutron Source of Argonne National Laboratory (ANL IPNS), with 150 meV incident energy and an energy window $0 \sim 200$ meV [84].

5.1 Data Analysis and Resolution

We show in Fig. 5-1, as an example, two complete sets (temperature series) of QENS area-normalized spectra. The broadening of the quasi-elastic peaks becomes more and more noticeable as temperature increases. In Fig. 5-1A, we may notice, from the shoulders of these spectral lines, that two groups of curves, $231 \sim 250$ K and $198 \sim$

209 K, are separated by the curve at a temperature of 220 K. This visual information reinforces the result of the detailed analysis shown in Figs. 5-3 and 5-4, that there is an abrupt dynamical transition at $T_L = 216$ K. Fig. 5-1B shows the RCM analysis of the spectrum taken at $T = 220$ K, close to the transition temperature. On the other hand in Fig. 5-1C, the spectra at pressure 1600 bar show a rather smooth variation with temperature, indicating that there is no sharp transition. This pressure corresponds to the end point of the line of F-S transitions shown in Fig. 5-7. Fig. 5-1D is, again, an RCM analysis of the spectrum taken at $T = 214$ K of this pressure. RCM, as one can see, reproduces well the experimental spectral line shapes of confined water. The broadening of the experimental data over the resolution function, shown in Figs. 5-1B and Fig. 5-1D, leaves enough dynamic information to be extracted by RCM.

In Fig. 5-2 we report the spectra collected at HFBS under 400 and 2000 bar pressures as well. The same behaviors as shown in Fig. 5-1 can be clearly seen in this figure as well.

5.2 Average Translational Relaxation Times

We have already shown that at ambient pressure, for hydrated MCM-41-S of pore size ≤ 18 Å, $\langle \tau_T \rangle$ exhibits a F-S transition with the same transition temperature T_L within error bars. In Figs. 5-3 and 5-4, we report the temperature variation of $\langle \tau_T \rangle$ for water molecules as a function of pressure. It is seen that the panels in Fig. 5-3 all show clearly a F-S transition from a VFT law: $\langle \tau_T \rangle = \tau_1 exp\,[DT_0/(T - T_0)]$, where D is a constant providing the measure of fragility and T_0, the ideal glass transition temperature, to an Arrhenius law: $\langle \tau_T \rangle = \tau_1 exp\,[E_A/RT]$, where E_A is the activation energy for the relaxation process and R, the gas constant. This transition, is the signature of a F-S dynamic transition predicted by Ito et al [77], and now extends into finite pressures. The transition temperature, T_L, as the crossing point of the VFT

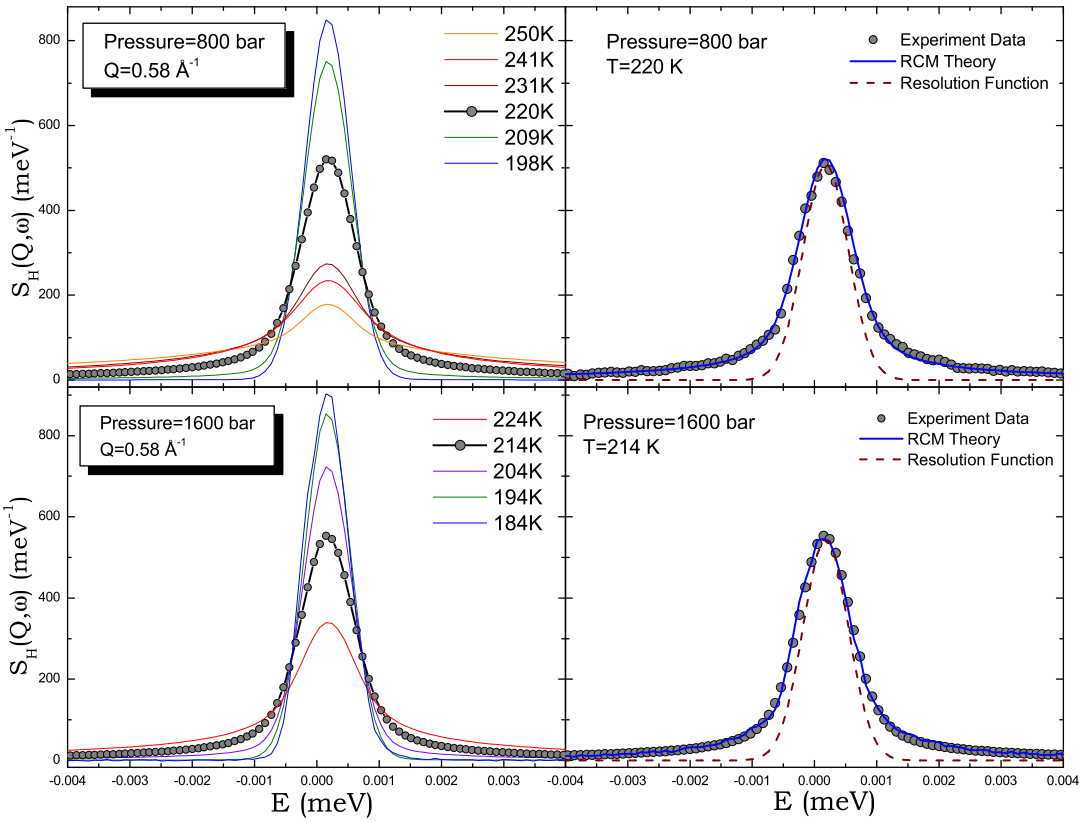

Figure 5-1: Figs. 5-1A and 5-1C (left panels) show QENS spectra measured at $Q = 0.58$ Å^{-1}, at two pressures, 800 bar and 1600 bar, and at a series of temperatures. Figs. 5-1B and 5-1D (right panels) show the RCM analysis of one of the spectrum from each pressure. The resolution function in each case is shown by a dashed line.

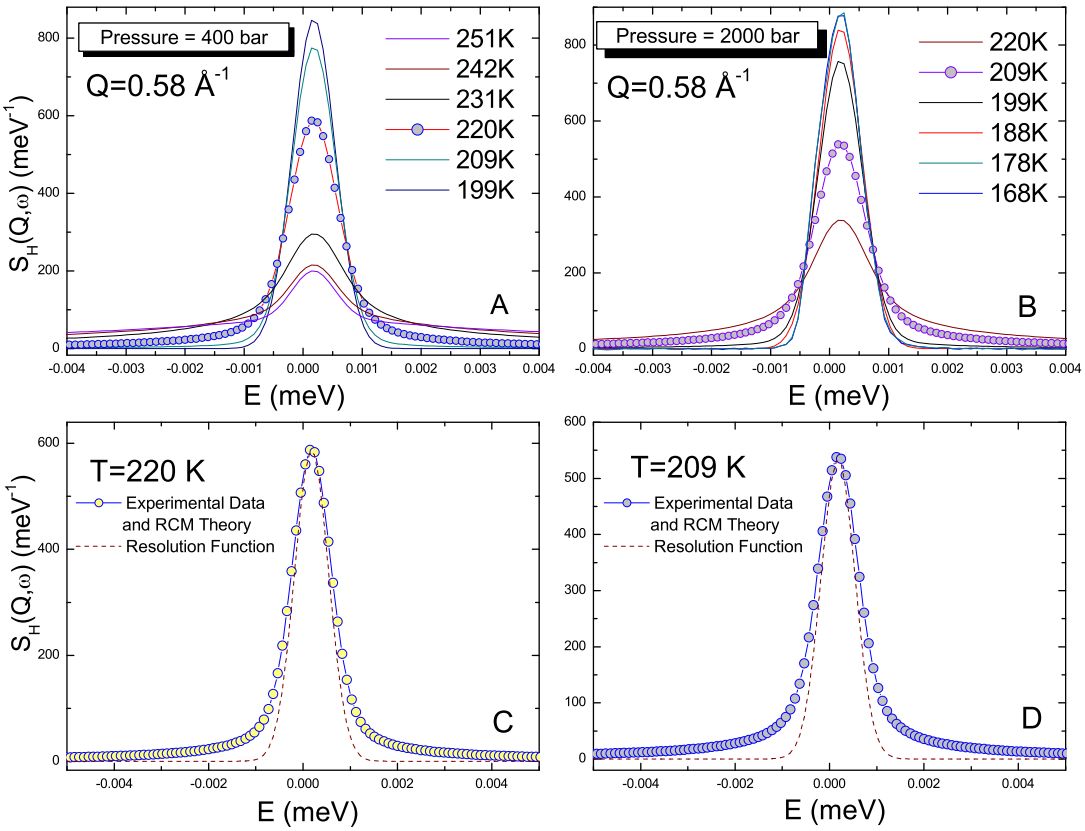

Figure 5-2: Top panels A and B show QENS spectra measured at $Q = 0.58\text{Å}^{-1}$, at two pressures, 400 bar and 2000 bar, and at a series of temperatures. Bottom panels C and D show the RCM analysis of one of the spectrum from each pressure. The resolution function in each case is shown by a dash line.

Table 5.1: F-S fitting parameters of experiments taken at high pressures, Sample: fully hydrated MCM-41-S-14.

Pressures (bar)	T_0 (K)	D	τ_1 (ps)	E_A $(Kcal/mol)$	T_L (K)
100	200	1.38	0.008	5.56	224
200	207	0.929	0.026	4.78	225
400	198	1.004	0.111	4.16	219
800	198	0.859	0.202	4.15	216
1200	189	1.05	0.097	3.94	210
1400	192	1.00	0.082	5.26	207

law and Arrhenius law, is calculated by $1/T_L = 1/T_0 - (Dk_B)/E_A$. All the parameters for the VFT and Arrhenius law fitting are reported in Table 5.1. However, in Fig. 5-4, the cusp-like transition becomes rounded off and there is no clear-cut way of defining the F-S transition temperature. Note that while we have done more experiments at high temperatures at 2000 bar pressure, shown in Fig. 5-4B, there is still a hint of fragile behavior at high enough temperature.

5.3 Other Results

Fig. 5-5 reports the temperature dependence of the product $\beta\gamma$ for pressure at 800 bar, as obtained from the fit. In the measured temperature range and similar to the one taken at ambient pressure [83], $\beta\gamma$, the actual exponent of the Q-dependence of the ISF, does not reach 2, as a free diffusion case, even at room temperature. The value of $\beta\gamma$ in Fig. 5-5 starts from a plateau value 1.3 at 320 K, close to the value for ambient pressure. Then it decreases gradually until $T \approx 210$ K and it reaches another plateau at about 0.7. This drop, not precipitously as that of ambient pressure, also signals a change of the dynamical behavior of water at 210 to 220 K, signifying that water is structurally arrested.

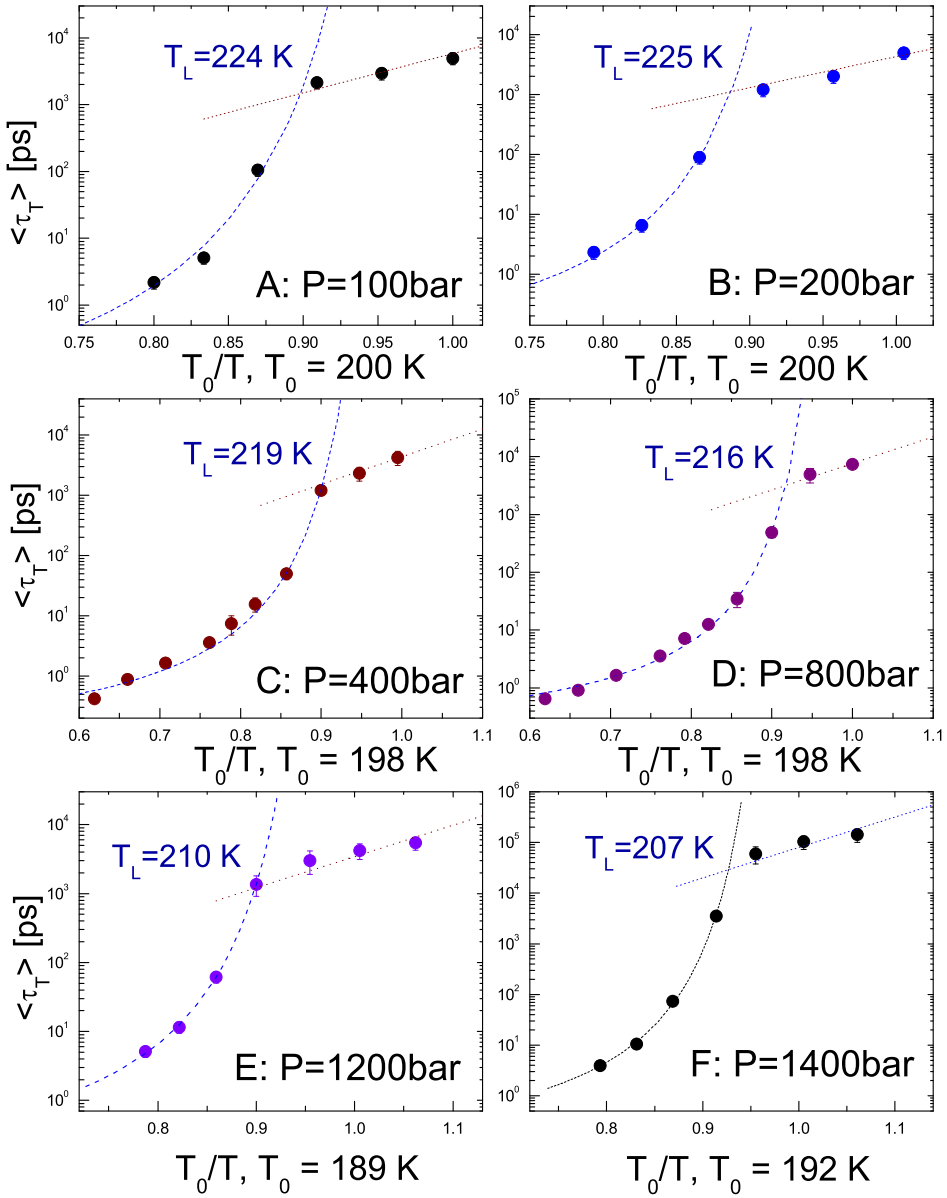

Figure 5-3: Temperature dependence of $\langle\tau_T\rangle$ plotted in $log(\langle\tau_T\rangle)$ vs T_0/T (or $1/T$) scale. Data from 100, 200, 400, 800, 1200, 1400 bars are shown in panels A, B, C, D, E, and F, respectively.

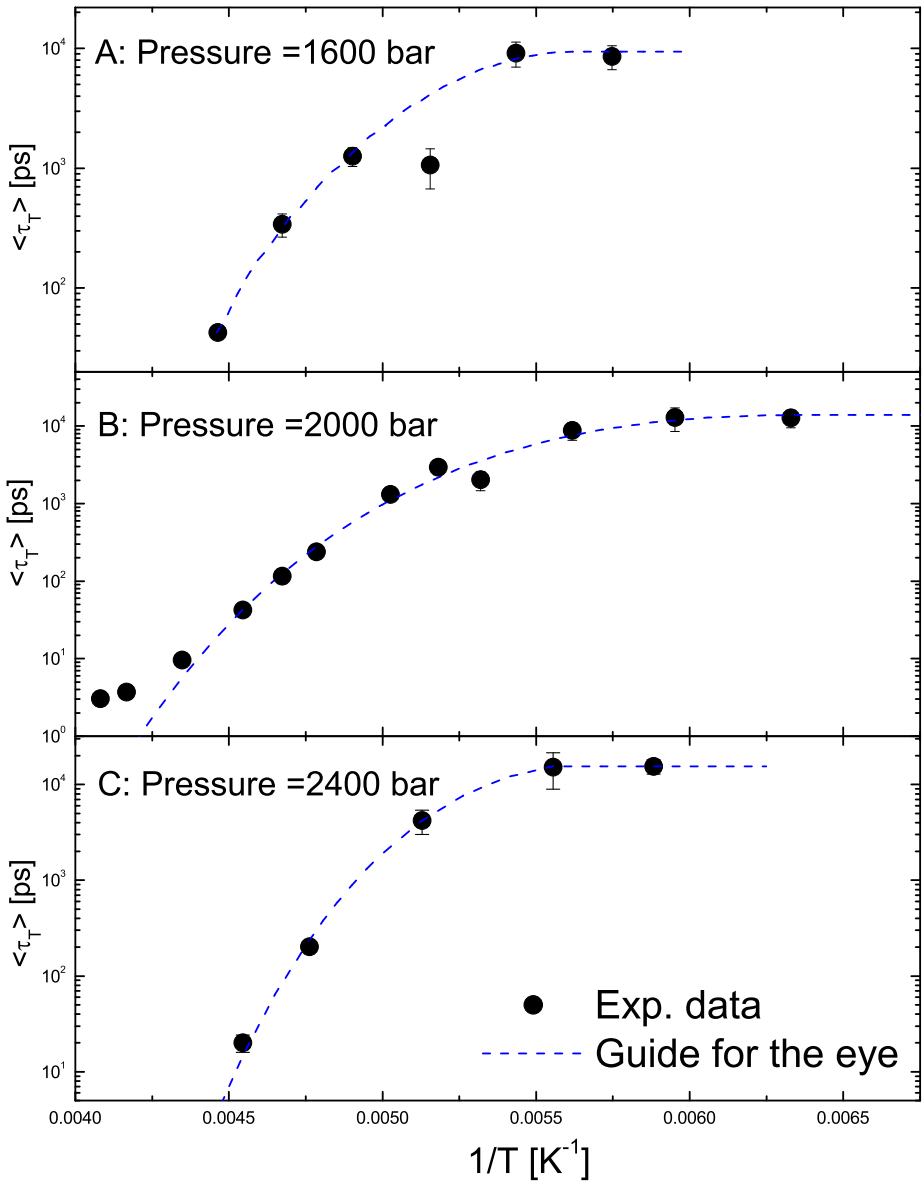

Figure 5-4: Temperature dependence of $\langle \tau_T \rangle$ plotted in $log(\langle \tau_T \rangle)$ vs $1/T$ scale. Data from 1600, 2000, and 2400 bars are shown in panels A, B, and C, respectively.

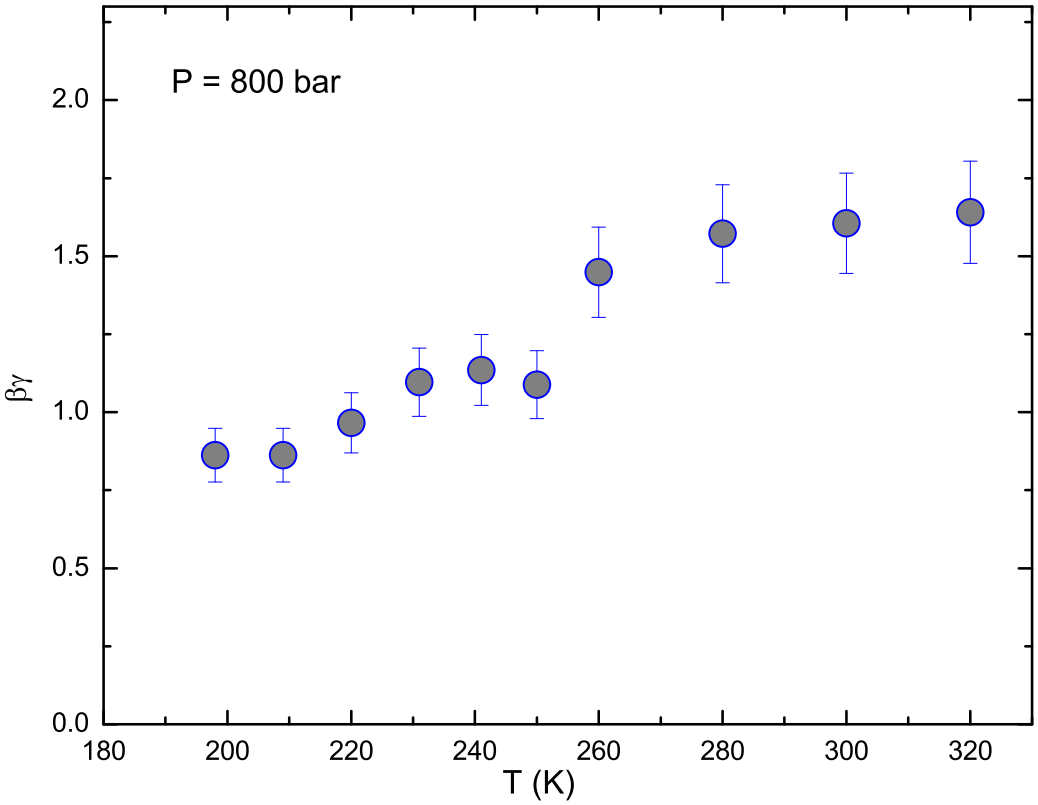

Figure 5-5: Temperature dependence of the product $\beta\gamma$ for pressure at 800 bar, where β is the stretch exponent, and γ, the translational relaxation time Q-dependence power law exponent.

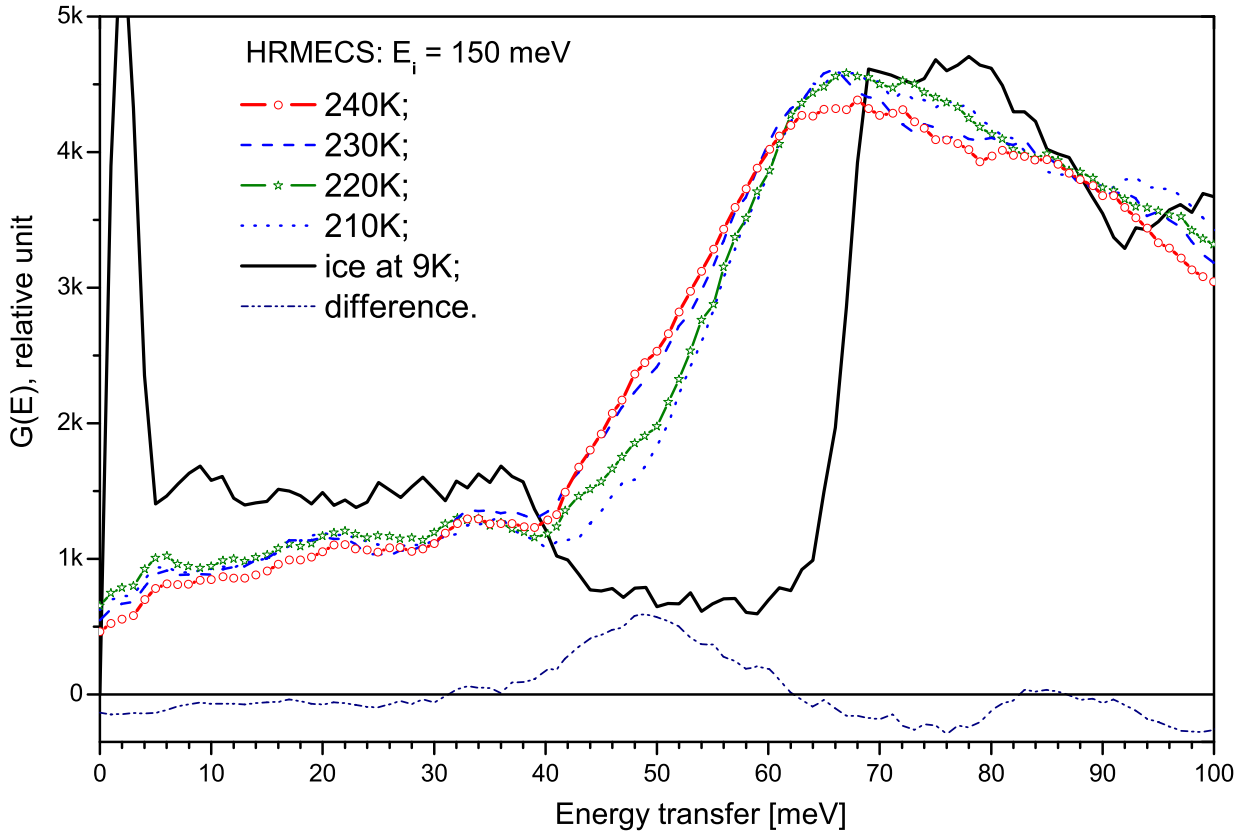

Figure 5-6: The generalized librational density of states G(E) (taken with $Q < 2$ Å^{-1}) of ice and confined water (within the energy range from 40 meV to 120 meV) at different temperatures measured with HRMECS spectrometer using incident neutron energy of 150 meV.

The HRMECS measurements were made on 55 wt% water in MCM-41-S with 18 Å pore size, and, in addition, on a bulk ice Ih at 9 K for comparison. Fig. 5-6 shows the observed vibrational density of states (DOS) of confined water at different temperatures as compared with those of ice Ih. It should be noted that G(E) of ice (solid line) is characterized by a much steeper leaning edge compared to those of supercooled water in the temperature range from 210 K to 240 K. The broader G(E)

of supercooled water confined in MCM-41-S with pore diameter of 18 Å is seen to be more characteristic of a liquid state. From the behavior of the low-energy cut-off of the librational band around 50 meV, it is obvious that the state of confined water (its hydrogen bond network) is different at temperatures above and below 225 K. The difference between the average spectra above and below 225 K is shown to have a clear peak at around 50 meV (dash-dot-dot line). It is obvious that the confined water does not transform into ice at all these temperatures. In addition, the figures from different temperatures form two groups, one below 225 K and another one above 225 K, with distinct gap in between. This behavior signals a structural change in the hydrogen-bond cage at 225 K.

5.4 Liquid-Liquid Transition and the Widom Line

According to the liquid-liquid phase transition hypothesis [1], to explain the anomalies of thermodynamic and transport properties of supercooled water, there is a first order phase transition line between two phases of liquid water: low-density liquid (LDL) and high-density liquid (HDL). This line is called Liquid-Liquid (L-L) transition line and terminates at a L-L critical point. It is to be noted that at lower pressure crossing the L-L transition line, the HDL and LDL phases are indistinguishable, just as the gas and liquid phases are indistinguishable above a liquid-gas critical point (refer to the $P - \rho$ diagram of superheated water, Fig. 2.2 of [85]). However, the L-L transition line extends into the one-phase region after terminating at the critical point [86]. This extended line, not being real, is the so-called Widom line. The Widom line is defined as a straight line in the Pressure-Temperature (P-T) plane, starting from the critical point C^* (p_C, T_C) and extending into the one-phase region, with the same slope as that of the L-L coexistence line at (p_C, T_C). Even though this line is an imaginary line, experiments of superheated water show that many thermodynamic quantities and transport coefficients, such as the isothermal compressibility, thermal-expansion coefficient, isobaric specific heat capacity, isochoric specific heat capacity, speed of sound, thermal conductivity, shear viscosity, and thermal diffusivity [85],

show a peak at the supposed crossing of the Widom line.

5.5 Discussions

Summarizing all the experimental results of fully hydrated MCM-41-S-14 under pressure, we show in a P-T plane, in Fig. 5-7 [87, 88], the observed pressure dependence of T_L and its estimated continuation, denoted by a dash line, in the pressure region where no clear-cut F-S transition is observed. One should note that the T_L line has a negative slope, parallel to TMD line, indicating a lower density liquid on the lower temperature side. This T_L line also approximately tracks the T_H line, and terminates in the upper end when intersecting the T_H line at 1600 bar and 200 K, at which point the character of the dynamic transition changes. We shall discuss the significance of this point later on. A special feature of the T_L line at the lower end should be noted as well. The line essentially becomes vertical after around 200 bar and the transition temperature approaches a constant value of $\sim$ 225 K.

Since T_L determined experimentally is a dynamic transition temperature, it is natural to question whether the system is in a liquid state on both sides of the T_L, and if so, what would the nature of the high-temperature and low-temperature liquids be? Sastry and Angell have recently shown by a MD simulation that at a temperature $T \approx 1060$ K (at zero pressure), below the freezing point 1685 K, the supercooled liquid silicon undergoes a first-order liquid-liquid phase transition, from a fragile, dense liquid to a strong, low-density liquid with nearly tetrahedral local coordination [89]. Prompted by this finding, we may like to relate, in some way, our observed T_L line to the liquid-liquid transition line, predicted by MD simulations of water [14] and speculating on the possible location of the low-temperature critical point.

According to our separate INS experiments, which measure the librational density of states of water contained in 18 Å pore size MCM-41-S, water remains in disordered liquid state both above and below the F-S transition at ambient pressure (Fig. 5-6). Furthermore, our analysis of the F-S transition for the case of ambient pressure indi-

cates that the activation energy barrier for initiating the local structural relaxation is $E_A = 4.89$ Kcal/mol for the low-temperature strong liquid. Yet, previous INS experiments of stretch vibrational band of water [90] indicate that the effective activation energy of breaking a hydrogen bond at 258 K (high-temperature fragile liquid) is 3.2 Kcal/mol. Therefore, it is reasonable to conclude that the high-temperature liquid corresponds to the high-density liquid (HDL) where the locally tetrahedrally coordinated hydrogen bond network is not fully developed, while the low-temperature liquid corresponds to the low-density liquid (LDL) where the more open, locally ice-like hydrogen bond network is fully developed [91].

It is appropriate now to address the possible location of the second critical point [14]. Above the critical temperature T_C and below the critical pressure p_C, we expect to find a one-phase liquid with a density ρ, which is constrained to satisfy an equation of state: $\rho = f(p, T)$. If an experiment is done by varying temperature T at a constant pressure $p < p_C$, ρ will change from a high-density value (corresponding to HDL) at sufficiently high temperature to a low-density value (corresponding to LDL) at sufficiently low temperature. Since the fragile behavior is associated with HDL and the strong behavior with LDL, we should expect to see a clear F-S transition as we lower the temperature at this constant p. Therefore, the cusp-like F-S transition we observed should then occur when we cross the so-called Widom line in the one-phase region [85]. On the other hand, if the experiment is performed in a pressure range $p > p_C$, corresponding to the two-phase region and crossing the L-L coexistence line, the system will be consisting of mixture of different proportions of HDL and LDL as one varies T. In this latter case, $\langle \tau_T \rangle$ vs. $1/T$ plot will not show a clear-cut F-S transition (the transition will be washed out) because the system is in a mixed state. The above picture would then explain the dynamical behavior we showed in Figs. 5-3 and 5-4. In Figs. 5-3 and 5-4, a clear F-S transition is observed up to 1400 bar and beyond 1600 bar the transition is rounded off. From this observation, the reasonable location of the L-L critical point is estimated to be at $p_C = 1600 \pm 200$ bar and

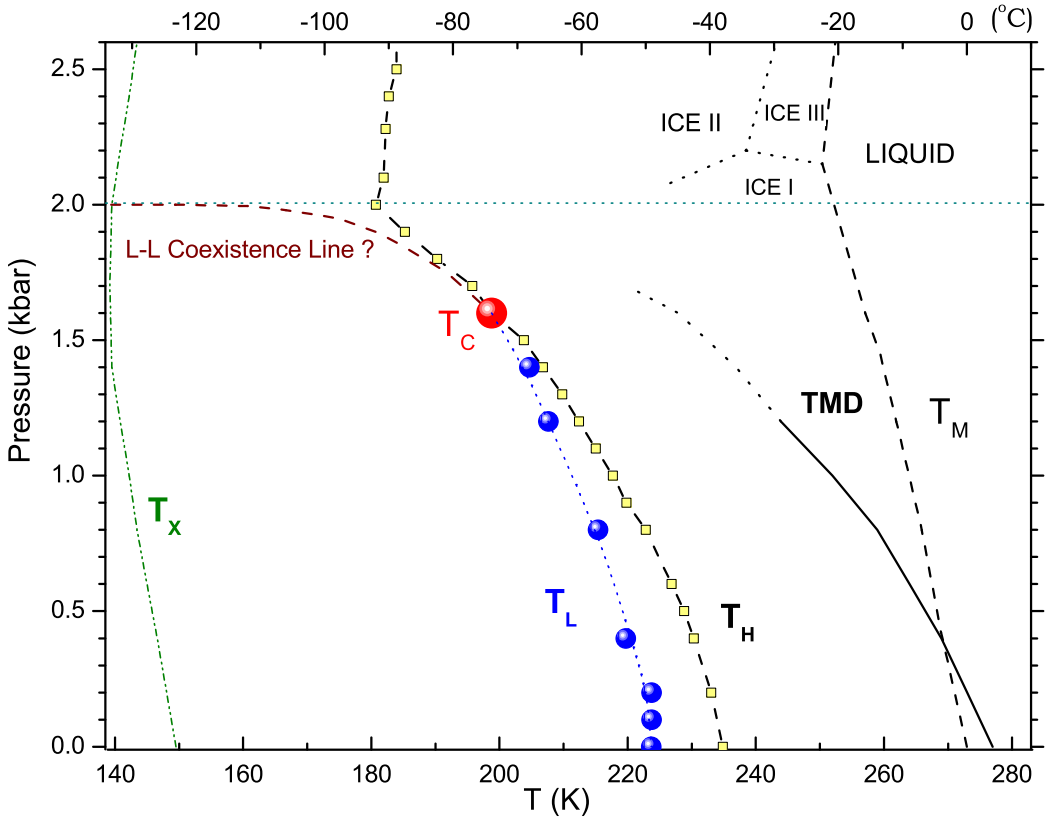

Figure 5-7: The pressure dependence of the F-T dynamic transition temperature, T_L, plotted in the P-T plane (solid circles). Also shown are the homogeneous nucleation temperature line, denoted as T_H, crystallization temperatures of amorphous solid water, denoted as T_X, and the temperature of maximum density line, denoted as TMD.

$T_C = 200 \pm 10$ K, shown by a big round point in Fig. 5-7.

Additionally, in a recent MD simulation using the Jagla Model Potential of Xu *et al* [92], a small peak was found in the specific heat C_P when crossing the Widom line at a constant p. Meanwhile, Maruyama et al conducted an experiment on adiabatic calorimetry of water confined within nano-pores of silica gel [93]. It was found that water within 30 Å pores was well prevented from crystallization, and also showed a small C_P peak at 227 K at ambient pressure. This experimental result further supports that the F-S transition we observed at 225 K at ambient pressure is caused by the crossing of the Widom line in the one-phase region above the critical point [92].

Moreover, we find that the long time dynamics of water below 200 bar becomes similar, as noted in Fig. 5-8. This special property may lead to another scenario that there is one more critical point lying in the negative pressure range, as was proposed by Brovchenko et al[1] [94]. Also, the critical point in the negative pressure was found in the case of the MD simulated liquid silicon quoted above [89], and with symmetric position in contrast with the one we show in Fig. 5-7 referring to the ambient (P, T) state point.

5.6 Contributions and Difficulties for the Past and Current Research

From mid-1990's, Chen et al brought up the idea of RCM to theoretically explain and fit QENS data. When I first entered the group, the theory for translational dynamics was almost done. Working closely with Prof. Chen, Ciya Liao, and Antonio Faraone, I then participated the completion of RCM, especially devoted to the rotational dynamics part of the model.

[1] Brovchenko et al studied supercooled water using Monte Carlo simulation with different potential models: TIP4P, TIP5P, and SPCE. All these models show two liquid-liquid phase transitions in supercooled region. This result suggests the possibility of water having two low-temperature critical points, one at positive pressure and the other at negative pressure.

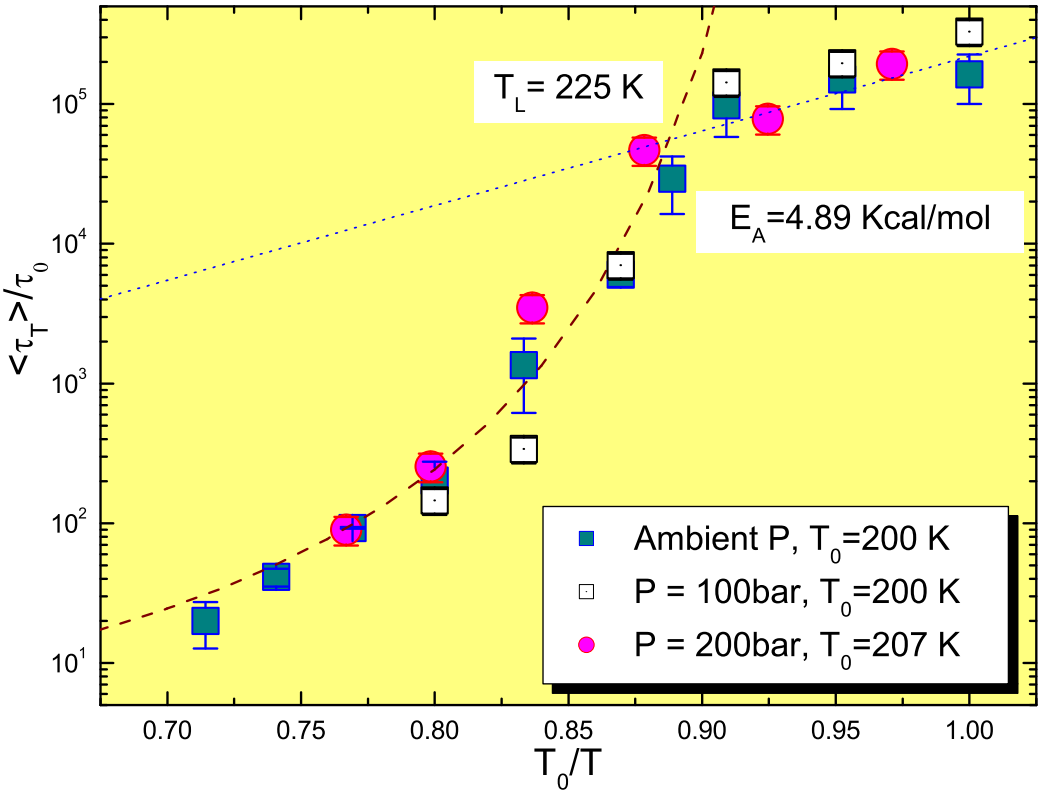

Figure 5-8: Scaling plot of $log(\langle\tau_T\rangle)$ vs T_0/T for data taken from 200, 100 and 1 bars. The fact that the three sets of data collapse into one master curve signifies that the slow dynamics becomes similar for pressures ≤ 200 bar. The VFT and Arrhenius law fit of the master curve gives the transition temperature $T_L = 225$ K and the activation energy $E_A = 4.89$ Kcal/mol.

The MD code attached with this thesis was borrowed from the previous work of F. Sciortino, P. Gallo, P. Tartaglia, and S.-H. Chen. Using this code, in past five years, we testified the validity of the RCM and did a series of simulation to predict the possible translational and rotational dynamics of supercooled water.

The QENS experiments were done at three different spectrometers: FCS, DCS, and HFBS at NIST NCNR. With a band of resolutions provided by the instruments themselves, it took us about a year to figure out which resolution and energy window to go with, at each spectrometer, for detecting the slow dynamics of supercooled water. Meanwhile, we used about two year time to scan through MCM samples with different pore sizes, and to wait for the pressure system to be built up.

Given all the theoretical and experimental basics and preliminary results, from about two years before, we finally focused our attention on the QENS experiments of MCM-41-S-14 under pressure. As shown before, each pressure was done with a series of temperatures, covering both below and above the transition temperature. Altogether, for only the pressure experiments, over 36 days of beam time[2] was used to measure about 1100 spectra, spanning 10 pressures: ambient, 100, 200, 400, 800, 1200, 1400, 1600, 2000, and 2400 bars.

However, the most difficult part of our research is to actually analyze the experimentally got data. We first generated the Fortran program (attached with this thesis) to fulfill the target of fitting QENS spectra with RCM model. Then we need to determine how many Q values are going to be fitted, by contrasting the resolution with the data taken. For the RCM analysis and for pressure experiments, we usually chose seven spectra, which stands for seven different Q values, for data taken at HFBS and eleven spectra for data taken at DCS, at each temperature[3]. The temperature dependence of the translational and rotational relaxation times[4] at each pressure is

[2]This 36 day beam time is extremely difficult to get from NIST NCNR and we are very thankful to Drs. E. Mamontov, J. R. D. Copley, I. Peral, Y. Qiu, and D. Neumann. Without their kind allocation of beam time and help during the experiments, we could not come up with our interesting results.

[3]In the case of ambient pressure, we have used the data from 11 (FCS), 9 (DCS), and 7 (HFBS) constant angle spectra. This was also reported in Chapter 3.

[4]Later we only take into account the translational relaxation time. For this part, please refer to Chapter 3 for "Low Q Approximation".

calculated from five fitted parameters, p, τ_0, γ, τ_R[5], and β, by analyzing a group of quasi-elastic peaks at different Q values simultaneously. After first round of fitting with free p, we determined the plateau value of elastic component p, fix its value and perform a second round of fitting all over[6]. It is to be known that the initial starting parameters affect the quality of fitting dramatically. Thus, in most times, to get reasonable error bars, reasonable converged τ_0, γ, τ_R, and β, we have to modify the starting values slowly and one by one.

It took us 16 months of CPU time of two computers to analyze the 1100 spectra, required for the identification of the fragile-to-strong transition at 10 pressures.

5.7 Perspective Future Research

Shown in Fig. 5-9, in terms of a contour plot of the $P(\rho, T)$ data as obtained by the MD simulation, is a recent proposed phase diagram of liquid supercooled water from study of Paschek [95]. This phase diagram apparently exhibits a first-order phase transition between two metastable liquid phases, ending in a second critical point C^*: $T^* = 210$ K, $P^* = 310$ MPa, and $\rho^* = 1.09$ g cm^{-3}. The location of C^* is somewhat close to the values reported by us: $p_C = 1600 \pm 200$ bar (160 ± 20 MPa) and $T_C = 200 \pm 10$ K. It is to be noted that the density goes through a minimum after the transformation into a low-density liquid state has taken place. Moreover, the difference between the density of HDL and LDL is small but significant, about 0.15 g cm^{-3}. Thus, while we try to testify our hypothesized second low-temperature critical point C^*, one important issue to be discussed next is the change of density. Neutron Diffraction (ND) method is an appropriate tool to detect the density of samples. We are ready to do ND experiments in the coming future. When the F-S transition happens dynamically at the temperature and pressure which supercooled confined water jumps from HDL phase into LDL phase, we would expect to see a drastic difference, from figures produced by ND, between the density before and after. In

[5]The parameter τ_R was excluded when $F_H(Q,t) \approx F_T(Q,t)$ at $Q \leq 1.1$ Å^{-1}. In this latter case, there are only four fitting parameters.

[6]The reason of doing this is explained in Chapter 3.

this way and compare the spectra we collect from a variety of pressures, we will then determine the existence of C^*.

A vastly broadened perspective on the liquid state has resulted from research initially aimed primarily at understanding polyamorphism in water [1]. It is well known that water molecules form a great variety of hydrogen bond networks, *i.e.*, pure water has many polymorphs, whose structures are varied by the interaction with other substances [96]. The structure and dynamics of water in a confined space, then, are modified by the presence of surfaces, by a change of hydrogen bonding but also by modification of the molecular motion that depends on the distance of water molecules from the surface. Therefore, a detailed description of these properties must take into account the nature of the substrate and its affinity to form bonds with water molecules, and the hydration level or number of water layers. In order to discriminate between these effects, reliable model systems exhibiting hydrophilic or/and hydrophobic interactions with water are required.

Recently, we have performed DCS experiments on fully hydrated single-walled carbon nanotube (SWNT), which has hydrophobic surfaces [97]. Also to be noted that the confinement we have used in the thesis MCM has hydrophilic surfaces. It will be, therefore, interesting to see the comparison of the $\langle \tau_T \rangle$ from supercooled water confined in hydrophilic MCM-41-S and hydrophobic SWNT. Showing in Fig. 5-10, we notice that the translational dynamics of H_2O confined in SWNT is much slower than that of H_2O confined in MCM, starting from room temperature. With the resolution of DCS, we cannot determine wether or not the F-S transition exists in H_2O/SWNT case. However, VFT law gives a reasonable fit to the $\langle \tau_T \rangle$ for $T \geq 200$ K. This result may lead to a lower T_L than that of H_2O/MCM-41-S-14 at ambient pressure, presumed that there is still an F-S transition.

Although a definitive picture of water's low-temperature dynamics and thermodynamics does not yet exist, the goal appears much closer now that it was. From our

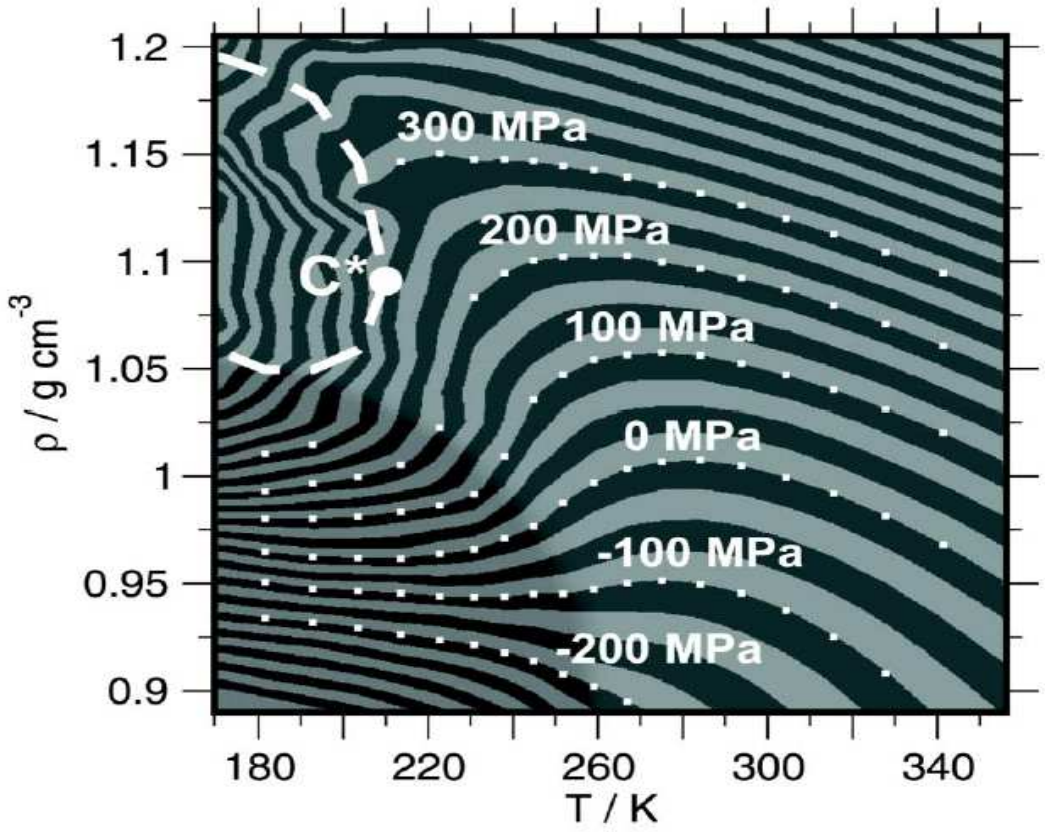

Figure 5-9: Phase diagram for stable and supercooled liquid TIP5P-E water. The spacing between different contour colors corresponds to a pressure drop of 25 MPa. Selected isobars are indicated. The heavy dashed line denotes the high density/low density liquid (HDL/LDL) coexistence line. The HDL/LDL critical point is located at C^* with $T^* = 210$ K, $P^* = 310$ MPa, and $\rho^* = 1.09$ g cm^{-3}. Darker shading indicated the LDL basin. This figure is taken from Fig. 1 of Ref. [95].

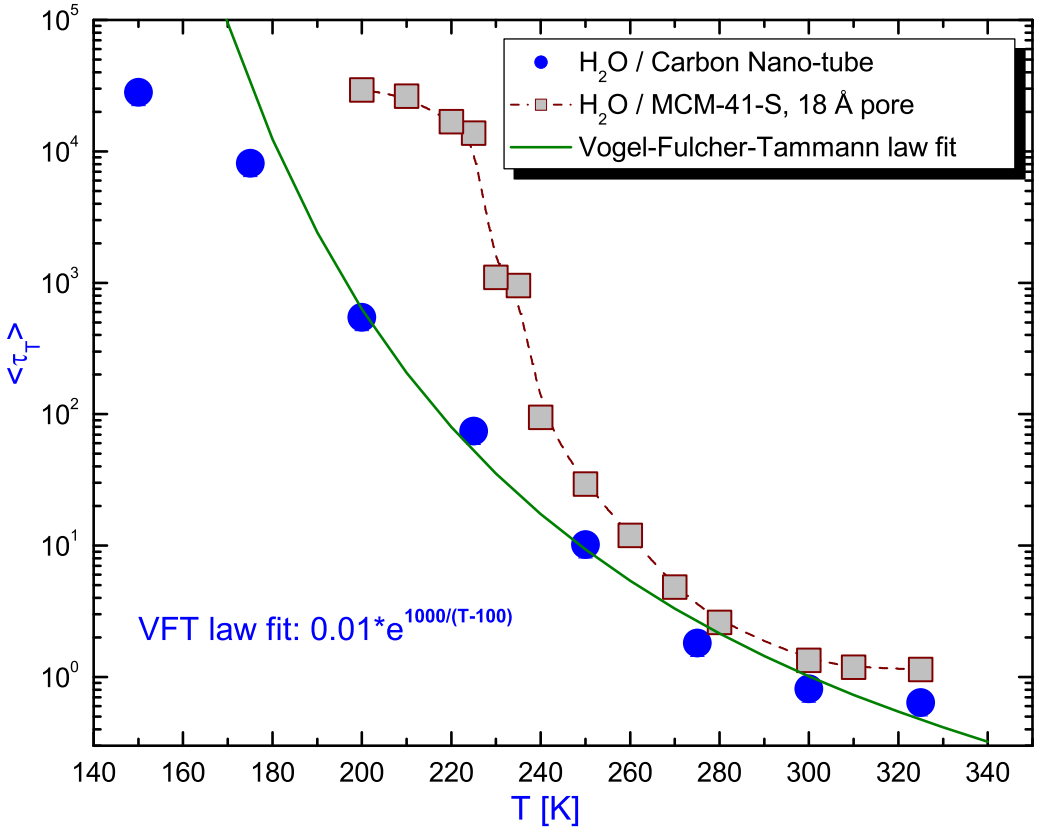

Figure 5-10: Temperature dependence of $\langle \tau_T \rangle$ plotted in $log(\langle \tau_T \rangle)$ vs T scale. Data from two different confinements: MCM-41-S and SWNT are shown by circles and squares, respectively. Also shown is the VFT law fit of $\langle \tau_T \rangle$ from the SWNT case. This experiment was done in collaborated with Dr. Alexander Kolesnikov at ANL IPNS.

QENS experiments and data analysis in this thesis, we have known that the F-S dynamic transition can be well detected for water confined in MCM-41 with pore sizes $\leq$ 18 Å and a possible second low-temperature critical point may be determined at this special case, fully hydrated H_2O/MCM-41-S-14. Whether or not the behavior we described above is general, no matter what kind of confinement we have, hydrophobic, hydrophilic, or somewhat in between, remains an intriguing and challenging topic, having tremendously impact as well.

That if the currently discussed hypothesis is correct could affect other fields of research in which the structure and dynamics of water are important [4]. In chemistry, the structure and properties of aqueous solutions [98, 99] might be viewed differently depending on the truthfulness of this hypothesis. In biology, the correct hypothesis may affect the explanation of the structure and reaction of the liquid water around biological macromolecules [100] and stereo-recognition of enzymatic processes [101]. Correct knowledge of the liquid state of water is also important for advancing the art of tissue cryopreservation [102]. Further, in chemical engineering, density and entropy fluctuations near the hypothesized second critical point might be important for aqueous reactions. Meanwhile, the structure of water is of particular interest in confined systems [103], such as the the clays that are of geological and biological interest. It has been speculated that polyamorphic transitions in liquid and amorphous solid water may occur inside (or on the surface of) icy bodies in space, and analogues of polyamorphic transitions have been proposed for the protein folding transition [104].

Fortunately, with the experimental tools we have right now, DCS method for high temperature dynamics, HFBS method for low temperature and 10 ns scale dynamics, and possible neutron spin echo method for extremely slow dynamics, and the applicable theoretical tool Relaxing-Cage Model, we are now ready to develop a definitive 'explanation' for the mysterious behavior of supercooled water in different confinements.

Coming next also to our agenda is to perform QENS experiments on a H_2O/deuterated protein system. Also to be done in the near future are more experiments on a H_2O/SWNT system and the research at the comparison of different hydration levels.

Through accomplishing the above study, we may modify our hypothesis by different substrate systems and hydration levels. And our continuous study may finally lead to a definitive picture of water's low-temperature dynamics and thermodynamics. And the well-known "No Man's Land" between 150 to 235 K shown in Fig. 9 of Ref. [105] may be filled with experimentally determined lines and points.

5.8 Conclusions

Water is essential for all living systems and the most abundant and important substance on Earth. Its properties impact our daily life and environment directly. Hence the counterintuitive behavior in its supercooled state stimulates enormous interests in condensed matter physics, physical chemistry and biophysics communities. For example, it expands rather than contracts with decreasing temperature, and some thermodynamic response functions and transport coefficients show a tendency to diverge at a singular temperature 228 K. However, this temperature is so-far inaccessible because water inevitably freezes into ice before reaching this temperature. By confining water in nano-pores of mesoporous silica MCM, we succeeded in entering this unreachable range of supercooled temperatures.

This thesis review our QENS studies of the dynamics of supercooled water confined in nanoporous silica materials. QENS data were analyzed by using RCM model previously developed by us. And the validity of RCM has been established by using MD simulation of SPC/E potential for bulk supercooled water, which applies to both the translational and rotational motion of water molecules. We then assume that the dynamics of water molecules in the vicinity of a hydrophilic surface is similar to a bulk water at an equivalent lower supercooled temperature. This analogy was experimentally demonstrated in previous investigations of water in vycor glasses and near hydrophilic protein surfaces. Studies were made of supercooled water in MCM-41-S and MCM-48-S using three QENS spectrometers at NIST NCNR at ambient pressure. Five quantities are extracted from the analysis: they are β, the stretch exponent characterizing the α-relaxation; $\beta\gamma$, the exponent determining the power-

law dependence of the relaxation time on Q; $\langle\tau_T\rangle$, Q independent pre-factor for the average translational relaxation time; $\langle\tau_{R_1}\rangle$, the relaxation time for the first-order rotational correlation function; and $\langle\tau_{R_2}\rangle$, the relaxation time for the second-order rotational correlation function. We discuss the temperature dependence of these parameters and noted in particular the dynamics is rapidly slowing down at the temperature around 225 K, signaling the onset of a structural arrest transition of liquid water into an amorphous solid water. An F-S dynamic transition has been detected for $\langle\tau_T\rangle$ happened at about 225 K.

Moreover, we studied the slow dynamics of supercooled confined water under various high pressures using HFBS and DCS at NIST NCNR. We observe clear evidence of a cusp-like F-S dynamic transition at pressures lower than 1600 bar. In the thesis, we show that the transition temperature decreases steadily with an increasing pressure, until it intersects the homogenous nucleation temperature line of bulk water at a pressure of 1600 bar. Above this pressure, it is no longer possible to discern the characteristic feature of the F-S transition.

This thesis elaborates our experimental findings of which the analysis, for the first time, elucidates the nature of the L-L transition line and Widom line, and suggests the location of the end point of L-L transition line, the much anticipated second critical point in recent literature.

Bibliography

[1] P.G. Debenedetti, and H. E. Stanley, Phys. Today **56**, 40 (June 2003).

[2] F. Franks, *Water: A Matrix of Life*, 2nd ed., Royal Society of Chemistry, Cambridge, UK (2000).

[3] P. Ball, *Life's Matrix: A Biography of Water*,Farrar, Straus, and Girous, New York (2000).

[4] O. Mishima, and H. E. Stanley, Nature **396**, 329 (1998).

[5] P. G. Debenedetti, *Metastable Liquids: Concepts and Principles*,Princeton U. Press, Princeton, N. J. (1996).

[6] H. E. Stanley, "Liquid and Glassy Water: Two Materials of Interdisciplinary Interest," S. Yip (ed.), 2005 *Handbook of Materials Modelilng*, (Springer, Printed in the Netherlands).

[7] R. J. Speedy, C. A. Angell, J. Chem. Phys. **65**, 851 (1976).

[8] C. A. Angell, J. Shuppert, J. C. Tucker, J. Phys. Chem. **77**, 3092 (1973).

[9] F. X. Prielmeier, E. W. Lang, R. J. Speedy, H.-D. Ldemann, Phys. Rev. Lett. **59**, 1128 (1987).

[10] Yu. A. Osipov, B. V. Zheleznyi, N. F. Bondarenko, Zh. Fiz. Khim. **51**, 1264 (1977).

[11] C. A. Angell, Ann. Rev. Chem. **55**, 559 (2004).

[12] P.G. Debenedetti, J. Phys.: Condens. Matter **15**, R1669 (2003).

[13] W. Gotze, L. Sjogren, Reports on Progress in Physics **55**, 241 (1992).

[14] P. H. Poole, F. Sciortino, U. Essmann, H. E. Stanley, Nature **360**, 324 (1992).

[15] R. Bergman and J. Swenson, Nature **403**, 283 (2000).

[16] S.-H. Chen and M.-C. Bellissent-Funel, in *Hydrogen Bond Networks*, Vol. 435 of *NATO Advances Study Institute, Series C: Mathematical and Physical Sciences*, edited by M.-C. Bellissent-Funel and J.C. Dore, 289 (Kluwer Academic, Dordrecht, 1994).

[17] J.-M. Zanotti, M.-C. Bellissent-Funel, and S.-H. Chen, "Water dynamics in the 'no man's land' temperature regime", to be published in Euro. Phys. Lett.

[18] M. Tarek, and D. J. Tobias, Phys. Rev. Lett. **88**, 138101 (2002).

[19] R. M. Lynden-Bell and J. C. Rasaiah, J. Chem. Phys. **105**, 9266 (1996).

[20] M. Settles and W. Doster, Faraday Discuss. Chem. Soc. **103**, 269 (1996).

[21] S.-H. Chen, C. Liao, F. Sciortino, P. Gallo, and P. Tartaglia, Phys. Rev. E **59**, 6708 (1999).

[22] L. Liu, A. Faraone, and S.-H. Chen, Phys. Rev. E **65**, 041506 (2002).

[23] P. Gallo, F. Sciortino, P. Tartaglia, and S.-H Chen, Phys. Rev. Lett. **76**, 2730 (1996).

[24] F. Sciortino, P. Gallo, P. Tartaglia, and S.-H Chen, Phys. Rev. E **54** 6331 (1996).

[25] S.-H. Chen, P. Gallo, F. Sciortino, and P. Tartaglia, Phys. Rev. E **56**, 4231 (1997).

[26] P. Gallo, M. Rovere, and E. Spohr, Phys. Rev. Lett. **85** 4317 (2000).

[27] P. Gallo, M. Rovere, and E. Spohr, J. Chem. Phys. **113**, 11324 (2000).

[28] S.H. Lee and P.J. Rossky, J. Chem. Phys. **100**, 3334 (1994).

[29] J.M. Zanotti, M.-C. Bellissent-Funel,and S.-H. Chen, Phys. Rev. E **59**, 3084 (1999).

[30] A. Botti, F. Bruni, A. Isopo, M.A. Ricci, and A.K. Soper, J. Chem. Phys. **117**, 6196 (2002).

[31] M.J. Benham, J.C. Cook, J.-C. Li, D.K. Ross, P.L. Hall, and B. Sarkissian, Phys. Rev. B **39**, 633 (1989).

[32] C. Rønne, P.-O. Åstrand, and S.R. Keiding, Phys. Rev. Lett.**82**, 2888 (1999).

[33] C. Rønne, and S.R. Keiding, J. Mol. Liq. **101**, 199 (2002).

[34] R. Bergman, J. Swenson, L. Børjesson, and P. Jacobsson, J. Chem. Phys **113**, 357 (2000).

[35] Y. Ryabov, A. Gutina, V. Archipov, and Y. Feldman, J. Phys. Chem. B **105** 1845 (2001).

[36] A. Gutina, T. Antropova, E. Rysiakiewicz-Pasek, K. Virnik, and Y. Feldman, Microporous and Mesoporous Materials **58** 237 (2003).

[37] F. D'Orazio, S. Bhattacharja, W.P. Halperin, K. Eguchi, and T. Mizusaki, Phys. Rev. B, **42**, 9810 (1990).

[38] S. Stapf, R. Kimmich, and R.-O. Seitter, Phys. Rev. Lett. **75**, 2855 (1995).

[39] J.P. Korb, J.-P. L. Malier, F. Cros, S. Xu, and J. Jonas, Phys. Rev. Lett. **77**, 2312 (1996).

[40] R. Holly, H. Peemoeller, C. Choi, and M.M. Pintar, J. Chem. Phys. **108** 4183 (1998).

[41] M.-C. Bellissent-Funel, S.-H. Chen, and J.M. Zanotti, Phys. Rev. E **51**, 4558 (1995).

[42] M.-C. Bellissent-Funel, S. Longeville, J.M. Zanotti, and S.-H. Chen, Phys. Rev. Lett. **85**, 3644 (2000).

[43] V. Crupi, D. Majolino, P. Migliardo, and V. Venuti, J. Phys. Chem. A **104** 11000 (2000).

[44] V. Crupi, D. Majolino, P. Migliardo, and V. Venuti, J. Phys. Chem. B **106** 10884 (2002).

[45] J. Swenson, R. Bergman, and W.S. Howells, J. Chem. Phys. **113**, 2873 (2000).

[46] J. Swenson, R. Bergman, and S. Longeville, J. Chem. Phys **115**, 11299 (2001).

[47] T. Takamuku, M. Yamagami, H. Wakita, Y. Masuda, and T. Yamaguchi, J. Phys. Chem. B **101**, 5730 (1997).

[48] S. Takahara, M. Nakano, S. Kittaka, Y. Kuroda, T. Mori, H. Hamano, and T. Yamaguchi, J. Phys. Chem. B **103**, 5814 (1999).

[49] F. Mansour, R.M. Dimeo, and H. Peemoeller, Phys. Rev. E **66**, 041307 (2002).

[50] S Mitra, R. Mukhopadhyay, I. Tsukushi, and S. Ikeda, J. Phys.: Condens. Matter **13**, 8455 (2001).

[51] P. C. Shih, H. P. Lin, C. Y. Mou, Stud. Surf. Sci. Catal., **146**, 557 (2003).

[52] Y. Liu, W. Zhang, T. J. Pinnavaia, J. Am. Chem. Soc. **122**, 8791 (2000).

[53] K. Schumacher, P.I. Ravikovitch, A. Du Chesne, A.V. Neimark, K.K. Unger, Langmuir **16**, 4648 (2000).

[54] Jackson, C. L.; McKenna, G. B. J. Chem. Phys. **93**, 9002 (1990).

[55] A. Meyer, R. M. Dimeo, P. M. Gehring, D. A. Neumann, Rev. Sci. Instrum. **74**, 2759 (2003).

[56] J. R. D. Copley, J. C. Cook, Chem. Phys. **292**, 477 (2003).

[57] P. Gallo, F. Sciortino, P. Tartaglia, and S.-H Chen, Phys. Rev. Lett. **76**, 2730 (1996).

[58] O. Steinhauser, Mol. Phys. **45**, 335 (1982).

[59] H. J. C. Berendsen *et al.*, J. Chem. Phys. **81**, 3684 (1984).

[60] E. Leuthesser, Phys. Rev. A **29**, 2765 (1984).

[61] U. Bengtzelius, W. Gotze, and A. Sjolander, J. Phys. C **17**, 5915 (1984).

[62] M. Fuchs, I. Hofacker, and L. Latz, Phys. Rev. A **45**, 898 (1992).

[63] W. Kob, and H. C. Andersen, Phys. Rev. E **51**, 4626 (1995).

[64] A. Faraone, S.-H. Chen, E. Fratini, P. Baglioni, L. Liu, and C. Brown, Phys. Rev. E **65**, 040501 (2002).

[65] A. Faraone, L. Liu, C.-Y. Mou, P.-C. Shih, J.R.D. Copley, and S.-H. Chen, J. Chem. Phys. **119**, 3963 (2003).

[66] A. Faraone, E. Fratini, P. Baglioni, and S.-H. Chen, J. Chem. Phys. **121**, 3212 (2004).

[67] S. W. Lovesey, *Theory of neutron scattering from condensed matter* (Oxford [Oxfordshire] : Clarendon Press, 1984).

[68] J. Teixeira, M.-C. Bellissent-Funel, S.-H. Chen, and A.J. Dianoux, Phys. Rev. A **31** 1913 (1985).

[69] K.E. Larsson, in *Thermal Neutron Scattering*, edited by P.A. Egelstaff, 347 (Academic Press, London, 1965).

[70] V. F. Sears, Can. J. Phys. **45**, 237 (1967).

[71] B.J. Berne, P. Pechukas, and G.D. Harp, J. Chem. Phys. **49** 3125 (1968).

[72] G. L. Squires, *Introduction to the Theory of Thermal Neutron Scattering*, Cambridge University Press. 1978.

[73] Allen S. Weinrub, *Cold Neutron Scattering by Molecular Liquids*, Ph. D thesis, Harvard University, 1971.

[74] L. Fabbian, F. Sciortino, and P. Tartaglia, J. non-cryst. solids **235-237**, 325 (1998).

[75] P. Gallo, F. Sciortino, P. Tartaglia, and S.-H Chen, Phys. Rev. Lett. **76** 2730 (1996).

[76] C. A. Angell, J. Non-Cryst. Solids **131-133**,13 (1991).

[77] K. Ito, C. T. Moynihan, and C. A. Angell, Nature **398**, 492 (1999).

[78] J. Colmenero, F. Alvarez, and A. Arbe, Phys. Rev. E **65**, 041804 (2002).

[79] A. Arbe, J. Colmenero, F. Alvarez, M. Monkenbusch, D. Richter, B. Farago, and B. Frick, Phys. Rev. Lett. **89**, 245701 (2002).

[80] J. Colmenero, A. Arbe, F. Alvarez, M. Monkenbusch, D. Richter, B. Farago, and B. Frick, J. Phys: Condens. Matter **15**, S1127 (2003).

[81] A. Faraone, L. Liu, and S.-H. Chen, J. Chem. Phys. **119**, 6302 (2003).

[82] V. Velikov, S. Borick, and C.A. Angell, Science **294**, 2335 (2001).

[83] A. Faraone, L. Liu, C.-Y. Mou, C.-W. Yen, and S.-H. Chen, J. Chem. Phys. **121**, 10843 (2004).

[84] C.-K. Loong et al., Nucl. Instr. Methods **A260**, 381 (1987).

[85] M. A. Anisimov, J. V. Sengers, and J. M. H. Levelt Sengers, Near-critical behavior of aqueous systems, in Aquesous Systems at Elevated Temperatures and Pressures: Physical Chemistry in water, Steam and Hydrothermal Solutions, D.A. Palmer, R. Fernandez-Prini and A.H. Harvey (Eds.), 2004 Elsevier Ltd.

[86] Private communication with L. Xu, S. Buldyrev, and H. E. Stanley. The authors wish to acknowledge conversations with these researchers on Mar. 27, 2005 when they drew our attention to this interpretation of the T_L line.

[87] L. Liu, S.-H. Chen, A. Faraone, C.-W. Yen, and C.-Y. Mou, "Pressure Dependence of Fragile-to-Strong Transition and a Possible Second Critical Point in Supercooled Confined Water," Phys. Rev. Lett. in press (2005).

[88] L. Liu, S.-H. Chen, A. Faraone, C.-W. Yen, C.-Y. Mou, A. Kolesnikov, E. Mamontov, J. Leao, "Quasielastic and inelastic neutron scattering investigation of fragile-to-strong transition in deeply supercooled water confined in nanoporous silica matrices," in preparation (2005).

[89] S. Sastry, C.A. Angell, Nature Materials **2**, 739 (2003).

[90] M.A. Ricci, S.-H. Chen, Phys. Rev. A **34**, 1714 (1986).

[91] A.K. Soper *et al*, Phys. Rev. Lett. **84**, 2881 (2000).

[92] L. Xu, P. Kumar, S.V. Buldyrev, S.-H. Chen, P. H. Poole, F. Sciortino, and H. E. Stanley, "Relation Between the Widom Line and the Fragility Transition" PNAS, in press (2005).

[93] S. Maruyama *et al*, AIP conference proc. **708**, 675 (2004).

[94] I. Brovchenko, A. Geiger, and A. Oleinikova, J. Chem. Phys. **123**, 044515 (2005).

[95] D. Paschek, Phys. Rev. Lett. **94**, 217802 (2005).

[96] M.-C. Bellissent-Funel, Eur. Phys. J. E **12**, 83 (2003).

[97] A. I. Kolesnikov, J. M. Zanotti, C. K. Loong, P. Thiyagarajan, A. P. Moravsky, R. O. Loutfy, C. J. Burnham, Phys. Rev. Lett. **93**, 035503 (2004).

[98] C. A. Angell, and E. J. Sare, J. Chem. Phys. **52**, 1058 (1970).

[99] R. Leberman, and A. K. Soper, Nature **378**, 364 (1989).

[100] P. M. Wiggins, Microbiol. Rev. **54**, 432 (1990).

[101] R. S. Phillips, J. Mol. Cat. B: Enz. **19 - 20**, 103 (2002).

[102] J. Dubochet, et al., Q. Rev. Biophy. **21**, 129 (1988).

[103] J. Dore, *Correlations and Connectivity*, eds: H. E. Stanley, and N. Ostrowsky, 188 (Kluwer Academic, Dordrecht, 1990).

[104] C. A. Angell, Physica D **107**, 122 (1997).

[105] H.E. Stanley, *Mysteries of Water*, M.-C. Bellissent-Funel(Ed.), the Nato Science Series A **305** (1999).

Appendix A

A List of Publications

• "Model for the rotational contribution to quasielastic neutron scattering spectra from supercooled water," L. Liu, A. Faraone, and S.-H. Chen, Phys. Rev. E **65**, 041506-1∼041506-8 (2002).

• "Rotational dynamics of hydration water in dicalcium silicate by quasielastic neutron scattering," A. Faraone, S.-H. Chen, E. Fratini, P. Baglioni, L. Liu, and C. Brown, Phys. Rev. E. Rapid Comm. **65**, 040501(R)-1∼040501(R)-4 (2002).

• "Dynamics of supercooled water in mesoporous silica matrix MCM-48-S," A. Faraone, L. Liu, C.-Y. Mou, P.-C. Shih, C. Brown, JRD Copley, RM Dimeo, and S.-H. Chen, Euro. Phys. J. E. **12**, S59∼S62 Suppl. 1 (2003).

• "Translational and rotational dynamics of water in mesoporous silica materials: MCM-41-S and MCM-48-S," A. Faraone, L. Liu, C.-Y. Mou, P.-C. Shih, JRD Copley, and S.-H. Chen, J. Chem. Phys. **119**, 3963∼3971 (2003).

• "Model for the translation-rotation coupling of molecular motion in water," A. Faraone, L. Liu, and S.-H. Chen, J. Chem. Phys. **119**, 6302∼6313 (2003).

• "Slow dynamics of supercooled water confined in nanoporous silica materials," L. Liu, A. Faraone, C.-Y. Mou, P.-C. Shih and S.-H. Chen, J. Phys.: Condens. Matter **16**, S5403∼S5436 (2004).

• "Dynamic Transition in Deeply Supercooled Water Confined in Nanoporous MCM-41-S," A. Faraone, L. Liu, C. Y. Mou, C.-W. Yen, and S.-H. Chen, J. Chem. Phys. Rapid Comm. **121**, 10843∼10848 (2004).

• "Pressure Dependence of Fragile-to-Strong Transition and a Possible Second Critical Point in Supercooled Confined Water," L. Liu, S.-H. Chen, A. Faraone, C.-W. Yen, and C.-Y. Mou, accepted and to appear in Phys. Rev. Lett. (2005).

• "Quasielastic and inelastic neutron scattering investigation of fragile-to-strong transition in deeply supercooled water confined in nanoporous silica matrices," L. Liu, S.-H. Chen, A. Faraone, C.-W. Yen, C.-Y. Mou, A. Kolesnikov, E. Mamontov, J. Leão, to be published (2005).

Appendix B

MD Simulation Code: SPC/E Potential (CD)

This program is incorporated in the attached CD.

Appendix C

Programs to Fit QENS Data by RCM (CD)

This program is incorporated in the attached CD.